

# *Ab initio* determination of thermal conductivity in crystals

Krzysztof Parlinski<sup>1,2</sup>

<sup>1</sup>*Institute of Nuclear Physics, Polish Academy of Sciences, Radzikowskiego 152, PL-31342 Kraków, Poland*

<sup>2</sup>*Computing for Materials, Kraków, Poland*

(\*Electronic mail: Krzysztof.Parlinski@ifj.edu.pl)

(Dated: 04 January 2023)

The calculations of thermal conductivity requires to know anharmonic properties of the crystal. For this purpose a non-perturbative anharmonic theory is applied, which do not make use of the potential energy expansion over atomic displacements, but instead, runs *ab initio* calculations of Hellmann-Feynman forces for atomic patterns of atoms with specific displacements to rebuild the anharmonic phonon frequencies, and group velocities. see [K.Parlinski, Phys.Rev. B **98**, 054305 (2018),] The Green-Kubo equation for the thermal conductivity needs to know the above quantities and the phonon relaxation times, which are related to the 4th-order phonon correlation function expressed in terms of phonon annihilation and creation Bose operators. In correct formulation of anharmonic theory the relaxation times can be derived as analytical expression. The Green-Kubo formulae was successfully applied to find thermal conductivity of *Si* and conductivities, related to the phonon and elastic waves, respectively, were computed.

## I. INTRODUCTION

The understanding of thermal conductivity in solids is needed for applications of technically relevant materials to nanofabrication technology, to manufacture electronic devices for nanoscale demands, to understand the mechanisms, predict the properties of solid thermal conductivities and to be able to run related computations. Similarly, handle of thermal conductivity describes partly the behaviour of thermoelectrics, electron-mediate superconductors and thermal conductivity materials, which govern the heat transfer processes in the Earth's interior.

The heat transport properties of solids are usually divided into two mechanisms: First kind is called **Lattice thermal conductivity** (LTC). It is calculated applying phonon anharmonicity. The method seems to be rather well known, and in this case the Green-Kubo linear-response theory<sup>1</sup> is mainly used. There are some variants in formulating this method. In one of them the harmonic phonon frequencies, the group velocities for phonon modes, and some relaxation times are used. Another way is to find the input data from the anharmonic perturbation method, usually with help of the triple and quatic order terms<sup>2-10</sup>, where relaxation time comes from solving the Boltzmann equation<sup>11,12</sup>, generally using third, or third and fourth order anharmonic terms only. Next method is to run molecular dynamics (MD)<sup>13-18</sup> provided that the potential of the studied system is known. The last mentioned approach solves the classical equations of motions for the system, tracing particle's evolution and then collecting the necessary quantities, which are required by Green-Kubo formulae. Typically, the Green-Kubo equations describe properly the thermal conductivity of solids for LTC, in the interval from around room to melting temperature. The anharmonic effects alone can be also studied applying the stochastic self-consistent harmonic approximation method<sup>19,20</sup>, which according to the Gibbs – Bogoliubov variational principle requires that the true free energy of the system reaches the minimum of the functional  $\mathcal{F}[\tilde{\rho}]$  with respect to all possible trial density matrices  $[\tilde{\rho}]$ .

The second kind of heat transport will be in this case called **High thermal conductivity** (HTC), for which the complete theory is still under construction. The HTC typically occurs in simple crystal structures. At *low temperature* (below 200 - 300K) HTC materials exhibit usually two, even three order of magnitude higher thermal conductivity values than the same material at high temperature range only (above 300K). To this group of crystals belongs: C (diamond), Si, Ge, AlN, AlP, BAs, BN, BP, BeS, GaN, MgO<sup>21</sup>. Thermal properties of several HTC crystals have been measured by Slack *et.al.*<sup>21-25</sup>. These HTC materials attracted special attention and called for relevant theory. In 1964 Glassbrenner and Slack<sup>25</sup> proposed a mechanism of HTC for silicon Si and Germanium Ge, based on phenomenological approach<sup>24,25</sup>. Later, a similar consideration on *ab initio* level was published by A.Ward *et.al.*<sup>12</sup>. Recently, Esfarjani *et.al.*<sup>26</sup>, studying Si, have discussed HTC mechanism as arising from large mean free path of phonons, determined by size of sample. It was shown that HTC of Si arises for more than order of magnitude, if mean free path spans from about nanometers to 100 microns.

It is generally accepted that the LTC is totally described by the acoustic and optic phonon modes, and therefore the LTC heat transfer is described by Green-Kubo formulae, where usually the relaxation time is found by Boltzmann equation or MD simulation. In articles<sup>27</sup> and<sup>28</sup> it was shown how the Green function of the anharmonic perturbation theory may lead to the typical Lorentzian term, with shift and width of anharmonic peak<sup>28</sup>.

In the article<sup>29</sup> it was attempted to decouple the fourth-order correlation function, responsible for the relaxation times and needed for thermal conductivity, using the pairing Wick's theorem, but finally MD runs validated the results for silicon.

In the present article we reformulate the Green-Kubo approach to use so called displacement patterns (DPs) of atomic configurations to derive the LTC directly from phonon dispersion curves created from DP and simultaneously determine phonon relaxation times. Moreover, derivation of the relaxation time from solution of the Boltzmann equation or MD calculations is not needed.

In next sections the method has been extended to handle also the HTC phenomena. In this case the low frequency and very long elastic waves are used to govern the HTC process. To calculate such long wavelength states we compute *ab initio* the elastic constant tensors with the equilibrium atoms in the supercell and for series of similar supercells with atoms displaced from equilibrium positions due to presence of temperature, like in DP. From these elastic supercells one calculates the frequencies and group velocities of the elastic waves, and apply them to the Green-Kubo expression to find HTC. In this case it is obvious that the accounted wavelength of elastic waves could be considerably longer than wavelength of ordinary phonons, therefore one must introduce limit to the longest active wavevector which could be accommodated in the sample size. The LTC and HTC calculation of Green-Kubo relations, as derived in this paper, have the same formal forms.

### A. Anharmonicity

The thermal conductivity in solids is determined by anharmonicity of the system, therefore, one should start from discussion how to handle anharmonicity. In present article a procedure, which takes also advantage of the *ab initio* calculations considers anharmonic properties of crystals within a new non-perturbative approach. (see Ref.<sup>30</sup>). It would be much easier to understand the current article first looking to Ref.<sup>30</sup> and glance at the examples presented there. There, the procedure begins from selecting the supercell of the studied crystal and calculating the harmonic phonons, using PHONON software<sup>31,32</sup>.

At equilibrium every atom of the crystal resides near the potential energy minimum. Displacing an atom from its equilibrium position by a vector  $\mathbf{u}$  one creates so called Hellmann-Feynman (HF) forces computed using VASP<sup>33</sup>, and acting on the surrounding atoms, in particular atoms of the supercell. PHONON computes in this way the harmonic phonon frequencies  $\omega^{(0)}(\mathbf{k}, j)$  and eigenvectors  $e^{(0)}(\mathbf{k}, j)$ . The HF forces could be calculated with the *ab initio* program. The same HF forces are used to build all force constants and dynamical matrix elements, which are the essential quantities in lattice dynamics theory since more as a century<sup>3</sup>. One should only keep in mind that the used atomic displacements amplitudes  $\mathbf{u}$  should probe only small interval of the harmonic potential around the atoms. From these data the mentioned software calculates harmonic phonon dispersion curves in the whole Brillouin zone. In the harmonic calculations the used atomic displacements  $\mathbf{u}$  are small, of order of 0.03 – 0.04 Å, which is close to zero-temperature phonon vibration.

In this harmonic theory<sup>30</sup> the method uses first the *exact* wavevectors  $\mathbf{k}$ , with wavelengths, being commensurate with the supercell size. At such *exact wavevectors*<sup>30-32</sup> the periodic structure of the crystals ensures that the harmonic frequencies  $\omega^{(0)}(\mathbf{k}, j)$  and eigenvectors  $e^{(0)}(\mathbf{k}, j)$  are calculated *exactly*, independent on the size of the supercell. Unfortunately, the list of exact wavevectors diminishes with decreasing size of the supercell. Of course, certain balance

between computational time and accuracy of the result will determine the selected supercell size. The phonon frequencies and eigenvectors beyond exact wavevectors are interpolations between exact wavevectors. The interpolations are supported by a traditional analytical derivation of dynamical matrix elements, which must be solved, what in practice leads to the valid results in the whole Brillouin zone. The interpolated procedure uses the singular value decomposition (SVD) method<sup>32,34</sup>, which simply assures that the finale phonon dispersion curves are the best fit in the mean square sense to the exact phonons frequencies of the exact points within the constraints of classical phonon dispersion curves. As a matter of fact this approach<sup>32</sup> to phonon theory was already equipped in 1996 with the procedure similar to the machine learning method.

The PHONON software<sup>30</sup> is also able to calculate the phonon dispersion curves from supercell with many atoms, which are displaced simultaneously out from their equilibrium positions. Moreover, if the atomic displacements stay small, it means they do not enter the non-parabolic part of the potential, then the resulting phonon dispersion curves look like in the harmonic case. Indeed, the force constants are determined by proportionality coefficient between atomic displacement and HF force and in harmonic regime do not depend on the amplitude of displacements.

However, if in the above procedure the displacements are larger, some deviation of the phonon frequencies might be observed because in reality atoms during vibrations visit the non-parabolic parts of the potential. These changes of frequencies and eigenvectors manifest the **anharmonicity**. Hence, the deviation of the particular phonon frequency ( $\omega^{(anh)}(\mathbf{k}, j) - \omega^{(0)}(\mathbf{k}, j)$ ), for the same  $(\mathbf{k}, j)$ , could be considered as a measure of the anharmonicity

Of course, it is well known that atoms vibrate in the crystal sites due to finite temperature  $T$ . For a given  $T$ , one should displace the atoms from their equilibrium positions and create the **displacements pattern (DP)** next used to find the phonon vibrations.

At a given  $T$ , the DP could be represented as a snapshot of supercell with many atoms displaced. One would like to create sets of  $N_i$  atomic displacement patterns DP<sup>(i)</sup>,  $i = 1, 2, \dots, N_i$ , which might arise in the crystal at a given  $T$ , and in different moments and locations. The proposition given in<sup>30</sup> is as follows: Each supercell DP should be filled with the phonon waves, determined by the well known expression of atomic displacements  $\mathbf{u}(\mathbf{m}, \mu, \gamma)$  and supplemented by the phase factor  $\phi(\mathbf{k}, j)$  of traveled phonon waves, where meaning of indices is later given before Eq.(8).

$$\mathbf{u}(\mathbf{m}, \mu, \gamma) = \frac{Q(\mathbf{k}, j)}{\sqrt{M_\mu}} e_{\gamma}(\mathbf{k}, j | \mu) \exp[2\pi i(\mathbf{k} \cdot \mathbf{R}(\mathbf{m}, \mu) - \phi(\mathbf{k}, j))] \quad (1)$$

The phase  $\phi(\mathbf{k}, j)$  of the phonon wave could be taken at random from the interval [0.0 – 1.0) to mimic different atomic displacement pattern labelled by the same  $(\mathbf{k}, j)$ . The mean square displacement amplitude  $\langle Q^2(\mathbf{k}, j) \rangle$  of the phonon wave was determined in<sup>35,36</sup> by

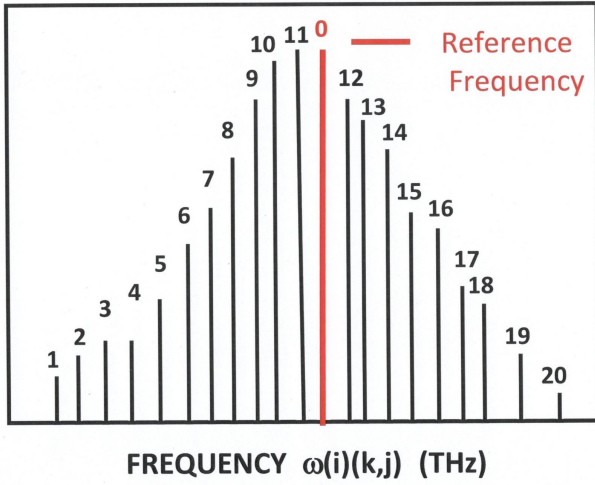


FIG. 1. A schematic set of  $DP^{(i)}$  in single anharmonic phonon peak.

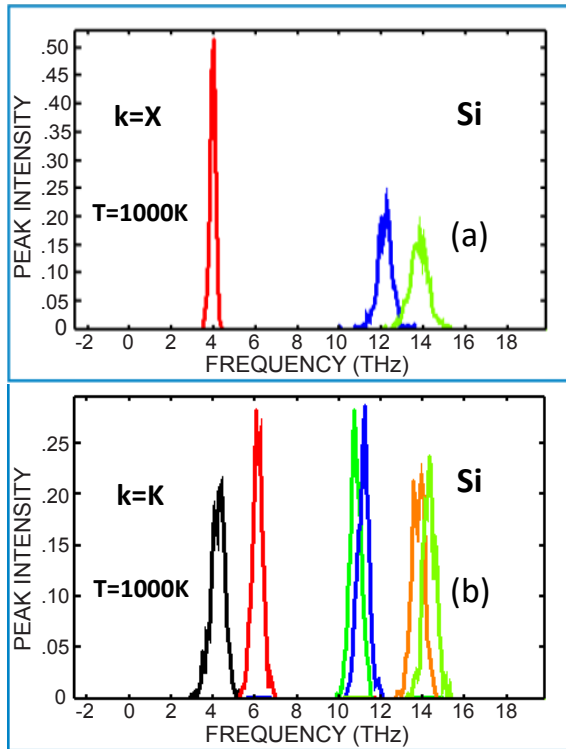


FIG. 2. Silicon *Si*. Anharmonic phonon peaks calculated for crystal at  $T = 1000K$  and wavevectors (a)  $X = (0.5, 0.5, 0.0)$  and (b)  $K = (0.375, 0.375, 0.725)$ . The plots arrived from  $DP^{(i)}$   $i = 1, 2, \dots, 500$ .

$$\langle Q^2(\mathbf{k}, j) \rangle = \frac{\hbar}{2\omega(\mathbf{k}, j)} \coth\left(\frac{\hbar\omega(\mathbf{k}, j)}{2k_B T}\right) \quad (2)$$

In the harmonic approximation the above relation is exact.

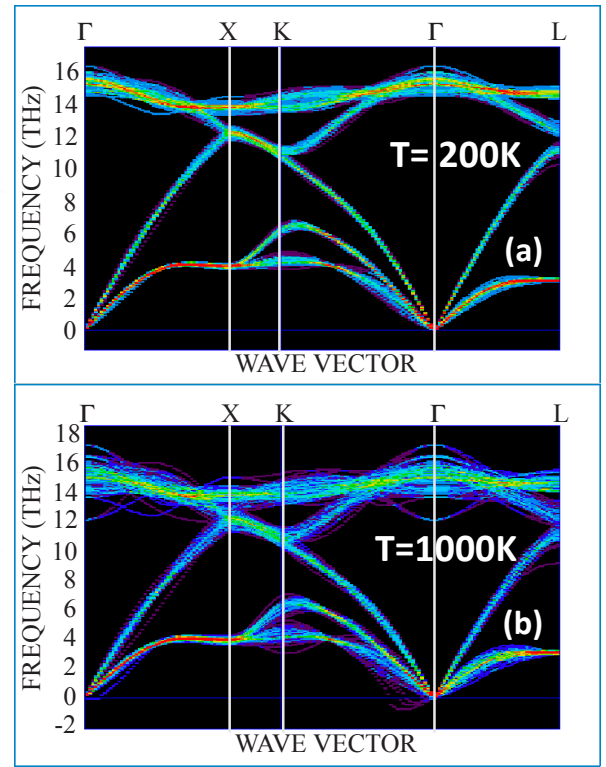


FIG. 3. Silicon *Si*. The maps of anharmonic phonon dispersion curves along the line of wavevector  $\Gamma - X - K - \Gamma - L$  for temperature (a)  $T = 200K$  and (b)  $T = 1000K$  calculated from  $DP^{(i)}$   $i = 1, 2, \dots, 500$  each. Blue-green-red colours indicates intensity.

<https://www.overleaf.com/project/63668958d1320f3c7c9a7540>

The *Si* and *MgO* the  $2 \times 2 \times 2$  supercell contains 64 atoms, 32 exact wavevectors each with 6 degree of freedom. Moreover, the phonon waves may still be supplemented by random number of phase  $\phi(\mathbf{k}, j)$  from the interval  $[0.0 - 1.0)$ . For *Si* and *MgO*, the atomic displacement changes with  $T$ , from Eq.(2), it follows  $Q = 0.05 - 0.16 \text{ \AA}$  in temperature range  $T = 40 - 1500K$ . This is only  $0.02 - 0.07\%$ , respectively, of the nearest neighbor interatomic distance.

Using the above method it is rather easy to obtain the anharmonic peaks for any wavevector  $\mathbf{k}$  and phonon branch  $j$ . These can be any wavevectors, although those which do not belong to list of exact wavevectors. One needs to create displacement patterns  $DP^{(i)}$ ,  $i = 1, 2, \dots, N_i$  in the range from  $N_i = 20$  to 500, depending on the requested precision. For conventional anharmonic peaks it could be limited to about  $N_i = 50$  DP, but to study a peculiar form of the anharmonic peak, such as asymmetric shape, particularly high background under the peak of non-Lorentzian shape, or even splitting of the single anharmonic peak, the value of  $N_i$  should be larger  $N_i = 200 - 500$ . The amplitudes of the vibrating atoms causing anharmonic effects and estimated above occur in real crystals and create many HF forces. These multiplicity of forces create multiplicity of force constants, which in turn, are used to solve the equations of classical lattice dynamic. Schematically the construction of anharmonic phonon mode can be

performed as shown on Fig.1. Examples of calculated anharmonic phonon peaks are shown on Fig.2. It is a set of  $\delta(\omega^{(i)})$  functions of  $DP^{(i)}1,2,i = \dots 20$ . Every segment  $i$  represents single snapshot of atomic displacements for the same anharmonic phonon mode. The phonon waves have different phases counting against the fixed sites of the atoms, hence the frequencies and intensities may vary a little. The  $\delta(\omega^{(i)})$  frequencies together with intensities (amplitude) are solutions of the lattice dynamic equations for the selected wavevector  $\mathbf{k}$  and accompanied displacements corresponding to temperature  $T$ . In the above scheme a set of 20  $\delta$ s mimic envelope of single anharmonic phonon mode. In further one calculation of anharmonic phonon mode with wavevector  $\mathbf{k}$  being located in between the already plotted one can be added to increase statistic and precision of phonon peak. The envelope of the delta set should give the form of the anharmonic peak. Reference frequency on the plot corresponds to harmonic frequency used later in the conductivity theory.

There appear more profits, following this method. Namely, in this theory *the symmetry* of each obtained anharmonic peak is uniquely labeled by the irreducible representation of the crystal space group. Normally, it is done only for the harmonic phonon  $\delta$ -kind peaks. Here, however, the calculated area under the anharmonic phonon peaks is characterized by the same irreducible representation.

From the same  $DP^{(i)}$ ,  $i = 1, 2, \dots N_i$ , with value  $N_i$  as discussed above, one may construct histograms for the phonon dispersion curves along any path of the reciprocal space, which next can be plotted as a map of the phonon dispersion curves. Such maps for Si at  $T = 200K$  and  $1000K$  are shown on Fig.3.

## B. Harmonic and anharmonic hamiltonians

The vibrational hamiltonian for a crystal in harmonic approximation<sup>3</sup> can be written as

$$H^{(0)} = \sum_{\mathbf{m},\mu,\gamma} \frac{P^{2,(0)}(\mathbf{m},\mu,\gamma)}{2M_{\mu}} + \frac{1}{2} \sum_{\mathbf{m},\mu,\gamma} \sum_{\mathbf{n},\nu,\delta} \Phi^{(0)}(\mathbf{m},\mu,\gamma;\mathbf{n},\nu,\delta) \times (U^{(0)}(\mathbf{m},\mu,\gamma)(U^{(0)}\mathbf{n},\nu,\delta)) \quad (3)$$

where the harmonic force constants  $\Phi^{(0)}$  have been calculated from the Hellman-Feynman forces of the perfect crystal with atoms preserving the crystal symmetry. The  $H^{(0)}$  hamiltonian describes the harmonic phonons. Solving the eigenvalue equation for  $H^{(0)}$  one arrives to harmonic phonon frequencies  $\omega^{(0)}(\mathbf{k}, j)$  and polarization vectors  $\mathbf{e}_{\mu}^{(0)}(\mathbf{k}, j)$ . These collection of harmonic phonons are used as a *reference set* of data when analysing the thermal conductivity.

The current method requires also to find phonon frequencies from the hamiltonians  $H^{(i)}$ , where "anharmonic" force constants  $\Phi^{(i)}$ ,  $i > 0$ , lead to larger/smaller displacement amplitudes, then in harmonic case. Now, one creates the Hellmann-Feynman forces for all displaced atoms collected

in  $DP^{(i)}$ , Eqs (1,2). Solution of these eigenvector equations leads to little different phonon frequencies and one may write

$$H^{(i)} = \sum_{\mathbf{m},\mu,\gamma} \frac{P^{2,(i)}(\mathbf{m},\mu,\gamma)}{2M_{\mu}} + \frac{1}{2} \sum_{\mathbf{m},\mu,\gamma} \sum_{\mathbf{n},\nu,\delta} \Phi^{(i)}(\mathbf{m},\mu,\gamma;\mathbf{n},\nu,\delta) \times (U^{(i)}(\mathbf{m},\mu,\gamma)(U^{(i)}\mathbf{n},\nu,\delta)) \quad (4)$$

If the anharmonic system converts to the harmonic one, then the force constants converge  $\Phi^{(i)} \rightarrow \Phi^{(0)}$ , and the forces are reduced to harmonic one. From the relations given above we conclude that in similar conditions as proclaimed above occurs  $H^{(i)} \rightarrow H^{(0)}$ , and therefore the anharmonic hamiltonians disappears  $H_A = 0$ . Anharmonic hamiltonian vanishes if the phonons of crystal become harmonic. Then, the thermal conductivity becomes infinity..

Above, the two body anharmonic force constants,  $\Phi^{(i)}(\mathbf{m},\mu,\gamma;\mathbf{n},\nu,\delta)$ , are labelled also by index  $(i)$  of  $DP^{(i)}$ , which indicates that the anharmonic force constant acting on the atom  $(\mathbf{m},\mu,\gamma)$  arises not only due to displacing a single atom  $(\mathbf{n},\nu,\delta)$  (as was in the harmonic case), but it really senses also forces coming from all other displaced atoms of supercell according to the configuration imposed by  $DP^{(i)}$ . This suggests that all atoms affects the anharmonic force constant  $\Phi^{(i)}(\mathbf{m},\mu,\gamma;\mathbf{n},\nu,\delta)$  as well. This means that  $\Phi^{(i)}(\mathbf{m},\mu,\gamma;\mathbf{n},\nu,\delta)$  is in some sense a many body force constant, which feels simultaneous displacements of all other atoms in the crystal. In other words all anharmonic force constants are computed not in the perfect crystal, but in the crystal being represented by a series of  $i = \dots$ , supercells, having atoms shifted out from equilibrium positions, due to finite temperature, and from that configuration one computes the contributions to anharmonicity.

The hamiltonian  $H^{(0)}$  provides harmonic phonon frequencies only. The harmonic potential for perfect insulator should lead to infinity thermal conductivity of the crystal. This statement has been expressed in the textbook of Ashcroft and Mermin<sup>37</sup>, in Callaway's<sup>11</sup> and Maradudin<sup>38</sup> papers. Ashcroft and Mermin says that "in perfect harmonic insulator crystal the phonon scattering does not occur, so such a crystal should have infinite thermal conductivity. Scattering of phonons from lattice imperfections would produce a finite thermal conductivity, but with a wrong temperature dependence. The only way to explain the realistic thermal conductivity data is to admit that phonons can be scattered by other phonons". Thus, the relevant thermal conductivity should exhibit the following properties: (i) demonstrate infinite thermal conductivity for strictly harmonic crystals. (ii) describe the finite thermal conductivity for crystal with anharmonicity. Consequently, one may propose to treat the thermal conductivity using the following approach. The anharmonic effects are described by the excess of effects arising from  $H^{(i)}$  hamiltonians, superimposed on the harmonic modes coming from  $H^{(0)}$ . Thus, the anharmonicity effects of a crystal can be determined by the

following hamiltonian

$$H_A = \frac{1}{N_i} \sum_{i=1}^{N_i} (H^{(i)} - H^{(0)}) \quad (5)$$

From the relations given above we may conclude that for vanishing anharmonicity, when  $H^{(i)} \rightarrow H^{(0)}$ , the anharmonic hamiltonians disappear  $H_A = 0$  and the crystal exhibits infinite thermal conductivity.

Because the hamiltonians  $H^{(0)}$  and  $H^{(i)}$ , Eqs(3,4) are sums of two positively definite quadratic forms, one in the components of the momenta and the other in the components of the atomic displacements, it follows from a theorem of matrix algebra<sup>39</sup> that it is possible to find principal axes, or normal coordinate transformations which simultaneously diagonalized the kinetic and potential energies in these hamiltonians. Such a principal axis transformations are generated by the conventional expansion of displacements and momenta in terms of plane waves and next Bose annihilation  $b(\mathbf{k}, j)$  and creation  $b^+(\mathbf{k}, j)$  operators.

In terms of these operators, the hamiltonians Eqs(3,4) take the simple forms

$$\begin{aligned} H^{(0)} &= \sum_{\mathbf{k}, j} \hbar \omega^{(0)}(\mathbf{k}, j) [b^+(\mathbf{k}, j)b(\mathbf{k}, j) + \frac{1}{2}] \\ H^{(i)} &= \sum_{\mathbf{k}, j} \hbar \omega^{(i)}(\mathbf{k}, j) [b^+(\mathbf{k}, j)b(\mathbf{k}, j) + \frac{1}{2}] \end{aligned} \quad (6)$$

From Eqs (5, 6) the anharmonic hamiltonian  $H_A$ , with subtracted harmonic phonon contribution  $H_0$  reads

$$\begin{aligned} H_A &= \sum_{\mathbf{k}, j} \sum_{i=0}^{N_i} (\hbar \omega^{(i)}(\mathbf{k}, j) - \hbar \omega^{(0)}(\mathbf{k}, j)) \\ &\quad \times b^+(\mathbf{k}, j)b(\mathbf{k}, j) \end{aligned} \quad (7)$$

where it has been assumed that the Bose operators  $b^+(\mathbf{k}, j)$  and  $b(\mathbf{k}, j)$  for the same mode  $(\mathbf{k}, j)$  with close frequencies should be, respectively, very similar and further we assume that they remain the same. Indeed, in this approach the anharmonicity is determined by the differences of  $(\hbar \omega^{(i)}(\mathbf{k}, j) - \hbar \omega^{(0)}(\mathbf{k}, j))$ .

These frequencies could be systematized and collected to histograms, labeled by a wavevector and phonon branch  $(\mathbf{k}, j)$  and finally to present as a Lorentzian-kind anharmonic peaks. Such peaks could be measured by inelastic neutron scattering, Raman spectra, or infrared absorption. Below we shall use this method to model the thermal conductivity as well. It is essential to remind that the path from the  $DP^{(i)}$  to phonon frequencies is performed by the solution of lattice dynamics equation of motion only.

Here, a single  $DP^{(i)}$  for fixed  $i$  can be treated as an anharmonic perturbation cluster, arising from simultaneously displacements of many atoms. In traditional perturbation theory,  $DP^{(i)}$  is typically limited to triple or quatic interactions. Here, a crystal with supercell of 64 atoms provides single  $DP^{(i)}$  data for all wavevectors  $(\mathbf{k}, j)$  of the Brillouin zone, so some cross interaction terms are included.

## II. FORMULAE FOR THERMAL CONDUCTIVITY

### A. Phonons

The Green-Kubo approach is based on statistical thermodynamics<sup>40-43</sup>. A derivation of basic formulae can be found in references<sup>8,26,44-46</sup>. The heat flux  $J(t)$ , for simplicity, is usually determined without contribution from diffusion and convection, (see Ref.<sup>8</sup>). Here also, we adapt the formalism of the anharmonic theory described in previous section, to apply the set of anharmonic hamiltonians  $H^{(i)}$  Eq.(5). The mentioned method expects the crystal to be presented as a set of  $N_i$  supercell's subsystems with atoms randomly displaced patterns  $DP^{(i)}$ ,  $i = 1, 2, \dots, N_i$ , corresponding to studied temperature  $T$ ,

$$\begin{aligned} J_\alpha^{(i)}(t) &= \frac{1}{2} \sum_{\mathbf{m}, \mu, \gamma} \sum_{\mathbf{n}, \nu, \delta} (R^\alpha(\mathbf{m}, \mu, \gamma) - R^\alpha(\mathbf{n}, \nu, \delta)) \\ &\quad \times \left( U^{(i)}(\mathbf{m}, \mu, \gamma | t) \cdot \bar{\Phi}^{(i)}(\mathbf{m}, \mu, \gamma; \mathbf{n}, \nu, \delta) \right. \\ &\quad \left. \cdot \frac{1}{M_\nu} P^{(i)}(\mathbf{n}, \nu, \delta | t) \right) \end{aligned} \quad (8)$$

Here, we use indexing of atoms: first atom:  $(\mathbf{m}, \mu, \gamma)$ , second atom:  $(\mathbf{n}, \nu, \delta)$ , where  $\mathbf{m}, \mathbf{n}$  are coordinates of primitive unit cells,  $\mu, \nu$  are atomic indices within primitive unit cells, and  $\gamma, \delta$  stay for coordinate  $x, y, z$ . The force constants  $\Phi^{(i)}(\mathbf{m}, \mu, \gamma; \mathbf{n}, \nu, \delta)$  may have contributions from harmonic and/or anharmonic regions of the interatomic potentials. In this sens the force constants may contain contributions from any higher order anharmonic terms. Moreover, the force constants might also have contributions from other displaced atoms of used  $DP^{(i)}$ , and not shown explicitly in the now discussed form of  $\Phi^{(i)}$ . The same force constant may also represent harmonic force constants.

As argued in Sec.IB the thermal conductivity should be calculated according to Eq.(9), over thermal fluctuations represented by the harmonic and anharmonic hamiltonians Eq.(5), determined by the components  $DP^{(i)}$  ( $i = 1, \dots, N_i$ ), all generated for the same  $T$ . The Green Kubo expression is then written as

$$\kappa_{\alpha, \beta} = \frac{1}{V k_B T^2} \frac{1}{N_i} \sum_{i=1}^{N_i} \int_0^\infty \langle J_\alpha^{(i)}(t) J_\beta^{(i)}(0) \rangle dt \quad (9)$$

Averaging the above correlation function over  $DP^{(i)}$  one may use it to study also anharmonic phonon peaks. Using the expansions of atom displacements and momenta over plane

waves  $Q^{(i)}(\mathbf{k}, j)$  and  $\dot{Q}^{(i)}(\mathbf{k}, j)$ , respectively,<sup>3</sup>, one has

$$\begin{aligned} U^{(i)}(\mathbf{m}, \mu, \gamma | t) &= \sqrt{\frac{\hbar}{NM\mu}} \sum_{\mathbf{k}, j} e_{\gamma}^{(i)}(\mathbf{k}, j | \mu) \\ &\times \exp[2\pi i(\mathbf{k} \cdot \mathbf{R}(\mathbf{m}, \mu))] Q^{(i)}(\mathbf{k}, j | t) \\ P^{(i)}(\mathbf{n}, \nu, \delta | t) &= \frac{1}{i} \sqrt{\frac{\hbar M \nu}{N}} \sum_{\mathbf{k}, j} e_{\delta}^{(i)}(\mathbf{k}, j | \nu) \\ &\times \exp[2\pi i(\mathbf{k} \cdot \mathbf{R}(\mathbf{n}, \nu))] \dot{Q}^{(i)}(\mathbf{k}, j | t), \end{aligned} \quad (10)$$

where (bold  $\mathbf{i} = \sqrt{-1}$ ),  $N$  is the number of wavevectors  $\mathbf{k}$  used in the summation of Eqs (10), and  $j$  is the index of phonon branches. Now, recalculating Eq.(8) one can rewrite it in the form

$$\begin{aligned} J_{\alpha}^{(i)}(t) &= \frac{\hbar}{iN} \sum_{\mathbf{k}, j} \omega^{(i)}(\mathbf{k}, j) \mathbf{v}_{gr}^{(i)\alpha}(\mathbf{k}, j) \\ &\times Q^{(i)}(\mathbf{k}, j | t) \dot{Q}^{(i)}(\mathbf{k}, j | t) \end{aligned} \quad (11)$$

Here, imaginary unit  $i$  appears since it was added to the exponent of the dynamical matrix  $D^{(i)}(\mathbf{k})$ , when used to define the group velocity, Eq(13)

In next steps one finds the phonon frequencies and eigenvectors for perfect crystal ( $i = 0$ ) and for crystal modified with DP ( $i$ ), ( $i > 0$ ). Both are lattice dynamic solutions of the eigenvalue phonon equation

$$\omega^{(i)2}(\mathbf{k}, j) = \mathbf{e}^{(i)T}(\mathbf{k}, j) \mathbf{D}^{(i)}(\mathbf{k}) \cdot \mathbf{e}^{(i)}(\mathbf{k}, j) \quad (12)$$

Of course they need different values of the elements of dynamical matrix  $D^{(i)}(\mathbf{k})$ .

Further, the group velocity vectors can be found from relevant dynamical matrices using

$$\begin{aligned} \mathbf{v}_{gr}^{(i)}(\mathbf{k}, j) &= \frac{1}{2\omega^{(i)}(\mathbf{k}, j)} \\ &\left[ \mathbf{e}^{(i)T}(\mathbf{k}, j) \left( \frac{\partial}{\partial \mathbf{k}} \mathbf{D}^{(i)}(\mathbf{k}) \right) \cdot \mathbf{e}^{(i)}(\mathbf{k}, j) \right] \end{aligned} \quad (13)$$

Notice that with the same equations the phonon frequencies  $\omega^{(i)}(\mathbf{k}, j)$  and group velocities  $\mathbf{v}_{gr}^{(i)}(\mathbf{k}, j)$  have been found in *ab initio* procedure via the Hellman-Feynman force<sup>30</sup> created by displacement of atoms fixed already in DP<sup>(i)</sup>'s. These deviations of DP<sup>(i)</sup> phonon frequencies from the relevant harmonic frequency contain information concerning the anharmonicity, in terms of frequency and eigenvectors.

Collecting the expressions of Eqs (9, 11, 13) the thermal conductivity tensor reads

$$\begin{aligned} \kappa_{\alpha, \beta}^{LTC} &= \frac{\hbar^2}{V_{puc} k_B T^2} \frac{1}{N_i} \sum_{i=1}^{N_i} \int_0^{\infty} dt \frac{1}{Nr} < \sum_{\mathbf{k}, j} (\omega^{(i)}(\mathbf{k}, j))^2 \mathbf{v}_{gr}^{(i)\alpha}(\mathbf{k}, j) \mathbf{v}_{gr}^{(i)\beta}(\mathbf{k}, j) \\ &\times < Q^{(i)}(\mathbf{k}, j | t) \dot{Q}^{(i)}(\mathbf{k}, j | t) \dot{Q}^{(i)}(\mathbf{k}, j | 0) Q^{(i)}(\mathbf{k}, j | 0) > \end{aligned} \quad (14)$$

where  $r$  is a number of atoms in primitive unit cell,  $V_{puc}$  volume of primitive unit cell. The appeared fourth order phonon correlation function  $< Q(t) \dot{Q}(t) \dot{Q}(0) Q(0) >$  needs some comments. It is the only function under the Laplace integral, which depends on time  $t$ . If the integrated function would be a constant  $C = const \neq 0$  then the Laplace integral  $\int_0^{\infty} C dt = \infty$ . This would be the mechanism to make a harmonic crystal having infinite thermal conductivity.

To considered the value of the fourth-order correlation function we need to express the normal mode amplitudes of phonons by Bose annihilation  $b$  and creation  $b^+$  operators

$$\begin{aligned} Q^{(i)}(\mathbf{k}, j) &= \frac{1}{\sqrt{2}} \frac{1}{\sqrt{\omega^{(i)}(\mathbf{k}, j)}} (b(\mathbf{k}, j) + b^+(-\mathbf{k}, j)) \\ \dot{Q}^{(i)}(\mathbf{k}, j) &= \frac{1}{\sqrt{2}} \sqrt{\omega^{(i)}(\mathbf{k}, j)} (b(\mathbf{k}, j) - b^+(-\mathbf{k}, j)) \end{aligned} \quad (15)$$

Now, the pair time-dependent correlation functions of  $b$ ,  $b^+$  are found from the solution of the Heisenberg time dependent equations<sup>3</sup>, in which the anharmonic hamiltonian  $H_A$  Eq.(5)

and (7) has been used. Then

$$\begin{aligned} &< b(\mathbf{k}, j | t) b^+(\mathbf{k}', j') | 0 > = \\ &\exp(-i\omega^{(i)}(\mathbf{k}, j) - \omega^{(0)}(\mathbf{k}, j)] t (n^{(i)}(\mathbf{k}, j) + 1) \delta_{\mathbf{k}, \mathbf{k}'} \delta_{j, j'} \\ &< b^+(\mathbf{k}, j | t) b(\mathbf{k}', j') | 0 > = \\ &\exp(+i\omega^{(i)}(\mathbf{k}, j) - \omega^{(0)}(\mathbf{k}, j)] t n^{(i)}(\mathbf{k}, j) \delta_{\mathbf{k}, \mathbf{k}'} \delta_{j, j'} \end{aligned} \quad (16)$$

Here, the mean number of phonons in the vibrational mode  $(\mathbf{k}, j)$  of DP<sup>(i)</sup> at temperature  $T$ , is

$$n^{(i)}(\mathbf{k}, j) = \frac{1}{e^{\beta \hbar \omega^{(i)}(\mathbf{k}, j)} - 1} \quad (17)$$

and  $\beta = \frac{1}{k_B T}$ .

Applying Eqs (15, 16), the fourth order correlation function  $< Q(t) \dot{Q}(t) \dot{Q}(0) Q(0) >$  can be evaluated, with the Wick' pairing theorem<sup>6,29</sup>, to 16 correlation functions of products of averages consisting of four  $b$ ,  $b^+$  operators each. In 10 functions, out of the mentioned 16, the 4 operator terms vanish due to averages build from pairs of the same kind of operators. The remaining 6 correlation functions do not vanish from the

mentioned reasons. However, 4 functions arrived from the last 6 non-zero terms, mutually cancel, due to averages build from pairs constructed from the same kind of operators and 6 terms are not vanishing from these reasons. However, the 2 last terms  $\langle b(t)b(t)b^+(0)b^+(0) \rangle$  and  $\langle b^+(t)b^+(t)b(0)b(0) \rangle$  remain non-zero and can be written as

$$\begin{aligned} & \langle b(\mathbf{k}, j | t)b(\mathbf{k}, j | t)b^+(\mathbf{k}, j | 0)b^+(\mathbf{k}, j | 0) \rangle = \\ & \quad 2(n^{(i)}(\mathbf{k}, j) + 1)^2 e^{-2i[\omega^{(i)}(\mathbf{k}, j) - \omega^{(0)}(\mathbf{k}, j)]t} \\ & \langle b^+(\mathbf{k}, j | t)b^+(\mathbf{k}, j | t)b(\mathbf{k}, j | 0)b(\mathbf{k}, j | 0) \rangle = \\ & \quad 2(n^{(i)}(\mathbf{k}, j))^2 e^{+2i[\omega^{(i)}(\mathbf{k}, j) - \omega^{(0)}(\mathbf{k}, j)]t} \end{aligned} \quad (18)$$

Applying the time dependence of the surviving pairs in Eq.(16), the non-zero fourth-order correlation functions are

$$\begin{aligned} & \langle Q^{(i)}(\mathbf{k}, j | t)\dot{Q}^{(i)}(\mathbf{k}, j | t)\dot{Q}^{(i)}(\mathbf{k}, j | 0)Q^{(i)}(\mathbf{k}, j | 0) \rangle = \\ & \quad (n^{(i)}(\mathbf{k}, j) + 1)n^{(i)}(\mathbf{k}, j) + 1/2) \times \\ & \quad \{ \cos 2(\omega^{(i)}(\mathbf{k}, j) - \omega^{(0)}(\mathbf{k}, j))t \} \\ & \quad - i(n^{(i)}(\mathbf{k}, j) + 1/2) \times \\ & \quad \{ \sin 2(\omega^{(i)}(\mathbf{k}, j) - \omega^{(0)}(\mathbf{k}, j))t \} \end{aligned} \quad (19)$$

The above correlation function shows real and imaginary components. The time dependence of the real one is governed by the cosine functions, which always have a maximum at  $t = 0$ . At increased time  $t$  the integrated functions, being the sum of many cosines with different periods will shrink to a bundle, which by increasing  $t$  finally converges to zero. Moreover, one may neglect  $1/2$  because its value appears to

be negligible in comparison to  $(n + 1)n$  in ranges of typical studied temperature.

The imaginary term contains periodic sine functions, which start from zero at  $t = 0$ . At finite values of  $t$  the sum of many sines with different signs and periods will lead the function shrinking around zero axis to zero bundle, making its contribution small. Consequently, we neglect the imaginary term as well.

Then, the final thermal factor appears to be equal to  $(n^{(i)}(\mathbf{k}, j) + 1)n^{(i)}(\mathbf{k}, j)$ , being the standard form occurring in the thermal conductivity expressions. It is the occupation coefficient responsible for the thermal distribution. Finally, the fourth-order phonon correlation function reads

$$\begin{aligned} & \langle Q^{(i)}(\mathbf{k}, j | t)\dot{Q}^{(i)}(\mathbf{k}, j | t)\dot{Q}^{(i)}(\mathbf{k}, j | 0)Q^{(i)}(\mathbf{k}, j | 0) \rangle = \\ & \quad \frac{1}{2} \left( (n^{(i)}(\mathbf{k}, j) + 1)n^{(i)}(\mathbf{k}, j) \{ \cos 2(\omega^{(i)}(\mathbf{k}, j) - \omega^{(0)}(\mathbf{k}, j))t \} \right) \end{aligned} \quad (20)$$

where the time dependence appears in a cosine function only. Then, the cosine argument consists of difference of two phonon frequencies. The first one come from DP<sup>(i)</sup>, which is the partial information of properties of the width of anharmonic peak  $(\mathbf{k}, j)$  in form of phonon frequency. The second is the reference frequency of the harmonic phonon from the same harmonic mode  $\omega^{(0)}(\mathbf{k}, j)$ . Below, we discuss the procedure to derive analytically the relaxation times for the thermal conductivity of anharmonic crystals directly from anharmonic theory<sup>30</sup>.

Let us insert the fourth-orders correlation function Eq.(20) into relation of the thermal conductivity Eq.(14). Within the current non-perturbative anharmonic approach<sup>30</sup> this would be the finale form of the general Green Kubo relation for thermal conductivity in crystals.

$$\kappa_{\alpha, \beta}^{LTC} = \frac{\hbar^2}{N r V_{puc} k_B T^2} \frac{1}{N_i} \sum_{i=1}^{N_i} \sum_{\mathbf{k}, j} (\omega^{(i)}(\mathbf{k}, j))^2 \mathbf{v}_{gr}^{(i)\alpha}(\mathbf{k}, j) \mathbf{v}_{gr}^{(i)\beta}(\mathbf{k}, j) \times (n^{(i)}(\mathbf{k}, j) + 1) n^{(i)}(\mathbf{k}, j) \times \frac{1}{2} \cos[2(\omega^{(i)}(\mathbf{k}, j) - \omega^{(0)}(\mathbf{k}, j))t] \quad (21)$$

## B. Relaxation Times of Phonon Modes

The last term of Eq.(21) is related to the relaxation function of the DP<sup>(i)</sup>

$$\tau_0^{(i)}(\mathbf{k}, j | t) = \frac{1}{2} \cos[2(\omega^{(i)}(\mathbf{k}, j) - \omega^{(0)}(\mathbf{k}, j))t] \quad (22)$$

After time-dependent Laplace integration one obtains a partial relaxation times (PRT)

$$\tau^{(i)}(\mathbf{k}, j) = \int_0^\infty \tau_0^{(i)}(\mathbf{k}, j | t) dt \quad (23)$$

Above partial relaxation time is labeled by phonon wavevector  $\mathbf{k}$ , phonon branch  $j$  and index  $(i)$  of DP<sup>(i)</sup>.

The conventional relaxation time (CRT), characterises the complete  $(\mathbf{k}, j)$  anharmonic phonon mode being a result of an average of all contributions from DP<sup>(i)</sup>. It reads

$$\begin{aligned} \tau_{con}(\mathbf{k}, j) &= \frac{1}{N_i} \sum_{i=1}^{N_i} \tau^{(i)}(\mathbf{k}, j) = \\ &= \frac{1}{2N_i} \sum_{i=1}^{N_i} \int_0^\infty dt \cos(2(\omega^{(i)}(\mathbf{k}, j) - \omega^{(0)}(\mathbf{k}, j))t) \end{aligned} \quad (24)$$

This is the relaxation time, which generally is used to calculate the thermal conductivity. The inverse of CRT is related to the width of the phonon anharmonic mode in frequency space.

To present the computed results of thermal conductivity we

selected out from general relations of Eq.(21), two auxiliary expressions (i) the time-independent amplitude function,

$$Z_{\alpha,\beta}^{(i)}(\mathbf{k}, j) = \left( \frac{k_B}{V_{puc}} \right) \left( \frac{\hbar \omega^{(i)}(\mathbf{k}, j)}{k_B T} \right)^2 \times \mathbf{v}_{gr}^{(i)\alpha}(\mathbf{k}, j) \mathbf{v}_{gr}^{(i)\beta}(\mathbf{k}, j) (n^{(i)}(\mathbf{k}, j) + 1) n^{(i)}(\mathbf{k}, j) \quad (25)$$

and (ii) time-dependent Kubo-Green function being the tensor of thermal conductivity function. This Kubo-Green functions have been plotted on many Figures of this article. Notice, that here averaging over index  $(i)$ , have not yet been applied.)

$$G_{\alpha,\beta}^{(i)}(t) = \frac{1}{N_r} \sum_{\mathbf{k}, j} Z_{\alpha,\beta}^{(i)}(\mathbf{k}, j) \tau_0^{(i)}(\mathbf{k}, j | t) \quad (26)$$

The above quantity averaged over DP $^{(i)}$  leads to averaged Green-Kubo components of the thermal conductivity tensor

$$\kappa_{\alpha,\beta}(t) = \frac{1}{N_i} \sum_{i=1}^{N_i} G_{\alpha,\beta}^{(i)}(t) \quad (27)$$

The Laplace integral over components of thermal conductivity tensor, Eq.(27) gives final tensor of the thermal conductivity. These quantity are given in Tables

$$\kappa_{\alpha,\beta} = \int_0^\infty dt \kappa_{\alpha,\beta}(t) \quad (28)$$

Finally, we define the global relaxation time (GRT). It is a common average relaxation time to characterize the whole studied system. It includes the Laplace integration, summation over all DP $^{(i)}$  and phonons  $(\mathbf{k}, j)$

$$\tau_{gl} = \frac{1}{2N_i N_r} \sum_{i=1}^{N_i} \sum_{\mathbf{k}, j} \int_0^\infty dt \cos(2(\omega^{(i)}(\mathbf{k}, j) - \omega^{(0)}(\mathbf{k}, j))t) \quad (29)$$

### III. LATTICE THERMAL CONDUCTIVITY

#### A. Displacement patterns for LTC

The above described theory will be applied to silicon *Si* and magnesium oxide *MgO*. These crystals belong to cubic structure with space groups  $Fd\bar{3}m$  and  $Fm\bar{3}m$ , respectively, and each with  $r = 2$  atoms per primitive unit cells. All the *ab initio* calculations have been performed using VASP software<sup>47</sup> on  $2 \times 2 \times 2$  supercells with periodic boundary conditions and 64 atoms. Using software PHONONA<sup>60</sup>, and calculating the Hellmann-Feynman forces created by VASP<sup>47</sup> the harmonic phonon dispersion curves  $\omega^{(0)} = \omega^{(0)}(\mathbf{k}, j)$ , were established and plotted. Next, these harmonic curves were used to create  $N_i$  number of DP $^{(i)}$  configurations with additionally randomly displaced atoms. All these DP have been used to create sets of the Hellman-Feynman forces, specific for each DP, created by relaxing the single electronic loop on VASP.

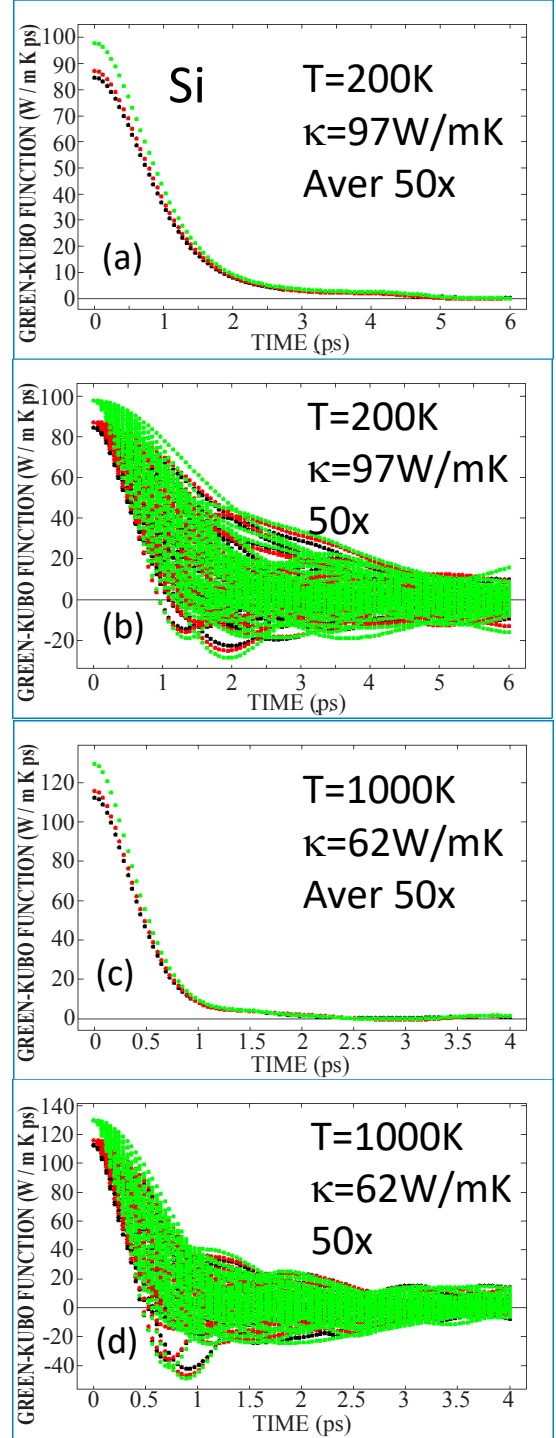


FIG. 4. Silicon, Si. Green-Kubo functions, (b,d), Eqs (21) (26), and averaged Green-Kubo functions, (a,c), Eq.(27). For lattice thermal conductivity and 50 DP.



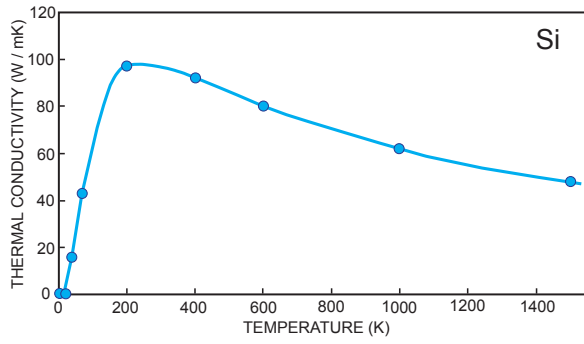


FIG. 5. Silicon Si. Lattice thermal conductivity, Eq.(21)

## B. Silicon LTC

At this point we may proceed a calculation of the LTC for Si using the DP determined in previous section. According to Eq.(21) these DP are used to average over  $i = 1, \dots, N_i$  the thermal conductivity. Phonon frequencies arising from  $N_i$  eigenvalue solutions, Eq.(12), can be plotted as phonon dispersion curves. The averages of the plotted curves reflect the magnitude of anharmonicity in any point of the Brillouin zone. They are just plotted on Fig.3 being results of 500 DP. One sees the broadening of anharmonic peaks with rising temperature. Notice that the same 500 DP could have been used to plot phonon dispersion curve, density of states, thermodynamic in anharmonic state and group velocities and LTC.

Using the formulae for thermal conductivity Eq.(21), the LTC has been calculated for temperatures  $T = 40, 70, 200, 400, 600, 1000, 1500K$ . The 50 DP were created for each temperature. During these procedures the lattice constant of  $a = 5.3847 \text{ \AA}$  was recorded, and we observed that the accompanied pressure was stabilized at about  $5.6kbar$ . However, due to somewhat lower accuracy of determined acoustic modes, the phonons having frequency below  $0.5THz$  were removed from contributing to atomic configuration, while creating DP patterns. Hence, low frequency phonons could be not sufficiently well represented at the low temperature region of thermal conductivity.

Fig.4b,d shows the detailed behaviour of the Green-Kubo functions, Eq.(26), for  $T = 200K$  and  $T = 1000K$  and for DP  $i = 1, \dots, 50$  diagonal components  $(\alpha, \alpha) = (xx, yy, zz)$ , plot from bottom to top in color order red, black, green. It is seen that the Green-Kubo functions are presenting some scatter, which at  $t = 0$  starts from value  $\frac{1}{N_r} \sum_{\mathbf{k}, j} Z_{\alpha, \beta}^{(i)}(\mathbf{k}, j)$ , then after a several  $ps$  becomes wide and tends at large  $t$  to a single line approaching infinity at  $G_{\alpha, \alpha}^{(i)}(t) = 0$ .

Fig.4a,c demonstrates that the global relaxation time for  $T = 200K$  and  $T = 1000K$  are about  $5.43ps$  and  $2.73ps$ , respectively, meaning that longer relaxation occurs at lower temperature. This figure, Fig.4a,c shows the global relaxation times plots, Eq.(29), being the averaged of Green-Kubo functions,  $G_{\alpha, \beta}(t)$ , Eq.(26), shows that the function really vanishes at larger time  $t$  values. In other words, the time dependent *cosines* periodic functions, which depend on different

TABLE I. Silicon Si and Magnesium Oxide MgO. Calculated averages of the sum  $\frac{1}{3}(\kappa_{1,1} + \kappa_{2,2} + \kappa_{3,3})$  of the lattice thermal conductivities Eq.(21), and the global relaxation times, Eq.(29).

Si $T(K)$	40	70	200	400	600	1000	1500
$\kappa(W/mK)$	15.8	43.1	96.8	92.4	79.8	61.6	47.5
$\tau(ps)$	5.94	5.89	5.43	4.40	3.66	2.73	2.11
MgO $T(K)$	20	100	300	600	1000	1500	
$\kappa(W/mK)$	3.14	49.3	110.2	92.2	68.3	50.9	
$\tau(ps)$	5,56	3.63	2.67	1.82	1.28	0.88	

phonon frequencies, will progressively overlap all terms so that at long  $t$   $G_{\alpha, \beta}(t) = 0$ . All diagonal  $xx, yy, zz$  components are computed, and the off-diagonal ones  $yz, xz, xy$  vanish due crystal symmetry and numerically.

Fig.4b,d shows, that the global relaxation time given in Table I for Si, diminishes with increased  $T$ . Moreover, the amplitude function  $Z_{\alpha, \beta}^{(i)}(\mathbf{k}, j)$ , Eq.(25), has been obtained in the same computational process as the global relaxation time  $\tau_{gl}$ . The  $\kappa_{\alpha, \beta}$  and  $\tau_{gl}$  decrease with increased temperature. The plot of computation silicon thermal behaviour of LTC is shown on Fig.5.

## C. Magnesium Oxide LTC

At this point we may proceed a derivation of the LTC for MgO with method described above. Applying the Eq.(21), using data of DP and related Hellman-Feynman forces coming from VASP, we determined the LTC coefficients for temperatures  $T = 20, 100, 300, 600, 1000, 1500K$ . The 50 DP were created for each mentioned temperature. The relaxing lattice constant was  $a = 4.2462 \text{ \AA}$ . The LO/TO splitting effect, present in MgO, was taken into account substituting values of ionic charges divided by electronic dielectric constant. The optical phonon branches, which depend on effective charges, are located at high frequencies and, as one should expect, have little influence on the thermal conductivity. The remaining calculation were performed in analogy to procedures used in Si, and described above.

Fig.6b,d shows examples of the detailed behaviour of the Green-Kubo functions, Eq.(26) for DP  $i = 1, \dots, 50$  for diagonal components  $(\alpha, \alpha) = (xx, yy, zz)$ , plot from bottom to top in color order red, black, green. It is seen that the Green-Kubo functions are somehow scattered. At  $t = 0$  they start from value  $\frac{1}{N_r} \sum_{\mathbf{k}, j} Z_{\alpha, \beta}^{(i)}(\mathbf{k}, j)$ , then after a time of several  $ps$  become wide and tends, at large  $t$ , to gather to a single line approaching infinity at  $G_{\alpha, \alpha}^{(i)}(t) = 0$ .

The relaxing lattice constant was  $a = 4.2462 \text{ \AA}$ . The thermal conductivity analysis were run for  $T = 20, 100, 300, 600, 1000, 1500K$ . The structure was stabilized at about  $10kbar$ . All  $N_i = 50$  DP were created with removed acoustic phonon modes below  $0.5THz$ . There was 192 exact wavevectors with the same exact point as for Si. The optical phonon branches, which dependent on effective charges, are located at high frequencies and, as one should expect, have

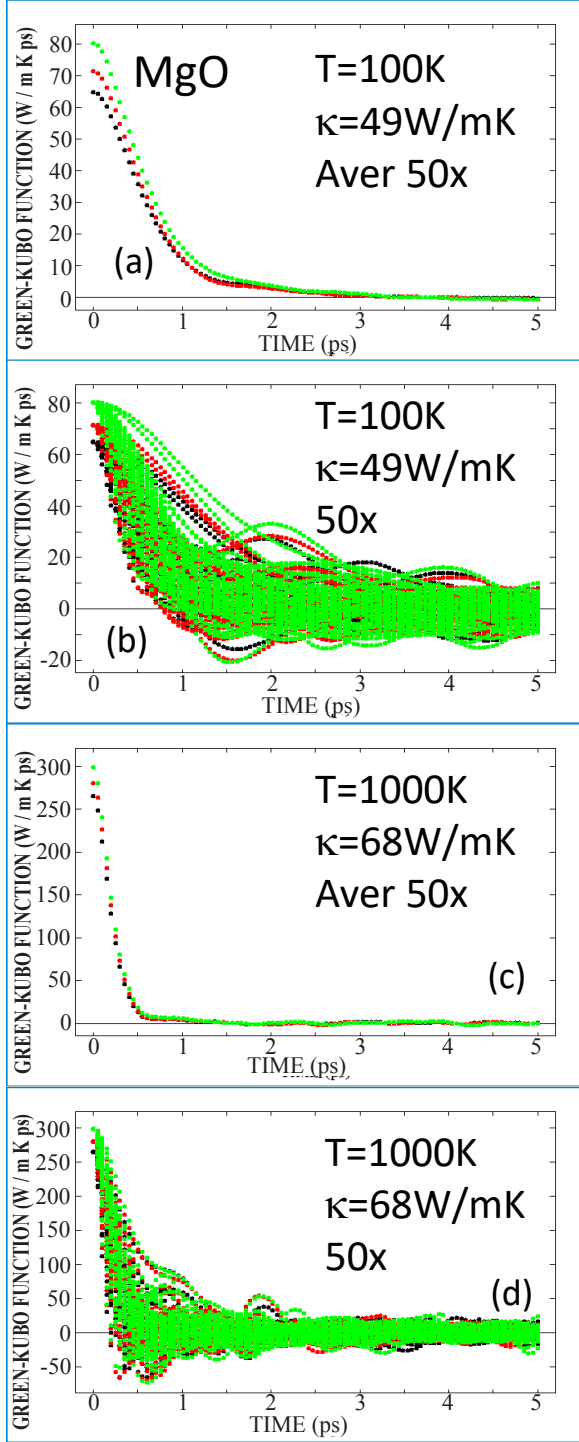


FIG. 6. Magnesium Oxide, MgO. Green-Kubo functions, (b,d), Eqs (21), (26), and averaged Green-Kubo functions, (a,c), Eq.(27). For lattice thermal conductivity and 50 DP.

little influence on the thermal conductivity. The remaining calculation were performed in analogy to procedures used in Si, and described above.

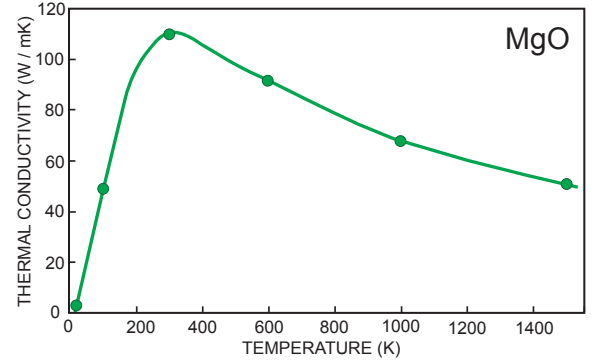


FIG. 7. Magnesium oxide, MgO. Lattice thermal conductivity, Eq.(21)

The Figs 6b,d and 6a,c show bundles of Green-Kubo  $G_{\alpha,\alpha}^{(i)}(t)$ , and averaged Green-Kubo functions the  $G_{\alpha,\alpha}(t)$ , respectively, Eq.(26). The figures for MgO look very similar to respective figures of Si. They also present the diagonal elements of the thermal conductivity tensors. The global relaxation times were estimated to be 3.63 ps and 1.28 ps for  $T=100K$ ,  $1000K$ , respectively. The temperature behaviour of LTC is shown on Fig.7. Similarly to Si, an abrupt decrease of LTC is observed below  $T = 200K$ .

#### IV. HIGH THERMAL CONDUCTIVITY

##### A. Elastic Tensor and Equation of Motion

A material with room-temperature thermal conductivity value larger than  $100 W/mK$  is regarded as a high thermal conductivity material<sup>1,21</sup>. Such an effect can be achieved either by extending the relaxation time  $\tau^{(i)}(\mathbf{k}, j)$ , or/and increasing of the amplitude function value  $Z_{\alpha,\beta}^{(i)}(\mathbf{k}, j)$ , Eq.(25). Here, we propose to justify the following approach, which might be able to provide high values of HTC.

It is well known that material temperature is mainly governed by its atomic vibrations, which perform vibrations with amplitudes of order  $0.01 - 0.20 \text{ \AA}$ . Such vibrations in form of the phonons occur in the whole crystal. Cooling/heating crystal causes to decrease/increase the atomic vibration amplitudes. For HTC, we are tempting to consider mainly the long, even very long vibrational waves, which do not care much on the atomistic details of the material structure. Then, the best is to use the elastic theory. Within the elastic theory it is convenient to determine supercell lattice as element of the crystal space, where the elastic waves would propagate. So elastic theory would allow to deform the supercell with no need to specified the atoms. In particular, one may study properties through the elastic tensor, which changes with deformations of supercell. One should, however remember that the elastic tensor is determined by the atomic interactions and atomic configurations.

There is another reason to pay attention to elastic wave

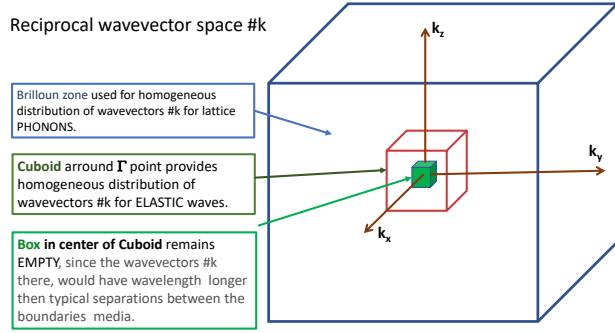


FIG. 8. (Color online) The *cuboid* volume to which are limited the wavevectors  $\mathbf{K}$  influencing the deformations of elastic constants tensors due to phonons displaced in the supercell by the presence of deformed elastic tensor (DET).

method. The HTC is determined by very long waves, having length even above microns. Such long acoustic phonons are usually represented as acoustic phonons. The frequencies of such acoustic phonons should be of very small and of very high accuracy, what frequently is difficult to achieve within lattice dynamics method alone, in particular in complex and low symmetry structures. A selection of elastic waves guaranties the correct values of elastic wave frequencies in vicinity of the  $\Gamma$  point. Indeed, sometimes in more complex crystals, the long acoustic phonons break the crystal symmetry due to their vibrations, generally guarantied by the translation-rotation invariances and dynamically violate the acoustic phonon properties. Therefore, it seems to be reasonable to replace the acoustic phonon modes by the elastic waves. The elastic waves diminish these effects. The elastic theory approach would operate with waves characterized by wavevectors of order  $\mathbf{k} = 0.5 - 0.000001 \text{ \AA}^{-1}$ , which cover the object sizes from nanometers- to microns. In this way one also may introduce the influence of material imperfections on the HTC thermal conductivity.

The equation of motion for elastic medium is formulated for elastic plane waves, which are written as

$$U(\mathbf{X}, t) = A_J \exp(\Omega(\mathbf{K}, J)t - \mathbf{K}\mathbf{X}) \quad (30)$$

where  $U_J(\mathbf{X}, t)$  is the supercell material deformation at point  $\mathbf{X}$  of the material, and  $J = 1, 2, 3$  is index of elastic mode. The  $A_J$  is a component of vibration amplitude,  $\Omega(\mathbf{K}, J)$  - angular frequency for elastic wave mode,  $t$  time, and  $\mathbf{K}$  the wavevector of monochromatic wave. The equation of motion of the elastic waves is called CHRISTOFFEL equation<sup>10,48-54</sup>

The Hooke's law relates the elastic strain  $\epsilon_{KL}$  with the stress  $\sigma_{IJ}$ .

$$\sigma_{IJ} = \sum_{K,L=1}^3 C_{IJKL} \epsilon_{KL} \quad (31)$$

where  $I, J, K, L$  are indices each from 1, 2 up to 3. The elastic properties of the material are described by a fourth-rank tensor  $C_{IJKL}$  with  $3^4 = 81$  elements. They can be arranged in a  $6 \times 6$

TABLE II. Contraction scheme: indices  $I, J, K, L$  in  $C_{I,J,K,L}$  are replaced by indices  $\alpha, \beta$  in  $C_{\alpha,\beta}$ . The same rules works in reverse direction. Scheme used by Voigt and VASP. The PHONONA uses VASP notation

I,J or K,L	11	22	33	23/32	13/31	12/21
$\alpha$ or $\beta$	1	2	3	4	5	6
Voigt	XX	YY	ZZ	YZ/ZY	XZ/ZX	XY/YX
VASP	XX	YY	ZZ	XY/YX	YZ/ZY	ZX/XZ

matrix that is symmetric, with elements  $C_{\alpha,\beta} = C_{\beta,\alpha}$ . The elastic tensor in the form of  $6 \times 6$  matrix should usually be available from external program like VASP.

$$C_{\alpha,\beta} = \begin{pmatrix} C_{11} & C_{12} & C_{13} & C_{14} & C_{15} & C_{16} \\ C_{21} & C_{22} & C_{23} & C_{24} & C_{25} & C_{26} \\ C_{31} & C_{32} & C_{33} & C_{34} & C_{35} & C_{36} \\ C_{41} & C_{42} & C_{43} & C_{44} & C_{45} & C_{46} \\ C_{51} & C_{52} & C_{53} & C_{54} & C_{55} & C_{56} \\ C_{61} & C_{62} & C_{63} & C_{64} & C_{65} & C_{66} \end{pmatrix}$$

The relations between  $C_{\alpha,\beta}$  and  $C_{JILM}$  are shown in Table II.

The stiffness tensor  $C_{\alpha,\beta}$  not only contains information about static materials deformation, but also about the elastic waves traveling through the material. The equation of motion for the elastic waves can be obtained from solution of the Christoffel equation<sup>48</sup>

$$\rho \Omega^2(\mathbf{K}, J) \cdot E(\mathbf{K}, J) = \sum_{I,L} K_I C_{JILM} K_L \cdot E(\mathbf{K}, M) \quad (32)$$

where  $\rho$  represents the mass density. The solution of the Cristoffel equation for each wavevector  $\mathbf{K}$  provides three solutions corresponding to elastic waves with definite frequencies. The equation combines the Cristoffel  $3 \times 3$  square matrix  $\mathbf{M}$  with elements

$$\mathbf{M}_{JM} = \sum_{I,L} K_I C_{JILM} K_L \quad (33)$$

Now, Eqs(32), and (33) form an eigenvalue problem that can be routinely solved at arbitrary  $\mathbf{K}$ . The result is a set of three frequencies  $\Omega^2(\mathbf{K}, J)$  and polarization vectors  $E(\mathbf{K})$ . Since  $\mathbf{M}$  is real and symmetric matrix, the eigenvalues are real and eigenvectors  $E(\mathbf{K}, J)$  constitute an orthogonal basis. Furthermore, the property that  $\mathbf{M}$  is a symmetric matrix involves that the  $\Omega^2(\mathbf{K}, J)$  is real and positive.

It is convenient to introduce auxiliary matrix

$$G_{J,M} = \sum_{I,L} K_I C_{JILM} K_L \quad (34)$$

This expression represents the core part of the Cristoffel Eq.(32). The derivatives of  $G_{J,M}$  are needed to specify the group velocity. They could be derived from three matrices of

order  $3 \times 3$ , which are wavevector derivatives of matrix  $G_{J,M}$

$$\begin{aligned}\Omega_0^2(\mathbf{K}, J) &= \text{Diag} \left[ \sum_{I,L} K_I C_{JILM} K_L \right] \\ \frac{\partial \Omega_0^2}{\partial K_x}(\mathbf{K}, J) &= \text{Diag} \left[ \sum_L (C_{J1LM} K_L + \sum_I K_I C_{JI1M}) \right] \\ \frac{\partial \Omega_0^2}{\partial K_y}(\mathbf{K}, J) &= \text{Diag} \left[ \sum_L (C_{J2LM} K_L + \sum_I K_I C_{JI2M}) \right] \\ \frac{\partial \Omega_0^2}{\partial K_z}(\mathbf{K}, J) &= \text{Diag} \left[ \sum_L (C_{J3LM} K_L + \sum_I K_I C_{JI3M}) \right]\end{aligned}\quad (35)$$

All matrices in Eqs (35) can be numerically diagonalized, which is marked by "Diag". The inputs are the right hand matrices, while the outputs constitute of following eigenvalues  $\Omega_0^2$ ,  $\frac{\partial \Omega_0^2}{\partial K_x}$ ,  $\frac{\partial \Omega_0^2}{\partial K_y}$  and  $\frac{\partial \Omega_0^2}{\partial K_z}$ . The diagonalization of the above matrices gives their eigenvalues. Moreover, one must also diagonalize the matrix  $G_{J,M}$ . Ratio of these data divided by 2 leads to the group velocities of the elastic waves. Furthermore, one might find this derivative differentiating the Cristoffel equation (32). From Eq.(32) one finds the group velocity of elastic waves

$$\mathbf{V}_{gr}(\mathbf{K}, J) = \frac{1}{2 \cdot \Omega_0(\mathbf{K}, J)} \left( \mathbf{i} \frac{\partial \Omega_0^2}{\partial K_x}, \mathbf{j} \frac{\partial \Omega_0^2}{\partial K_y}, \mathbf{k} \frac{\partial \Omega_0^2}{\partial K_z} \right) \quad (36)$$

$$\begin{aligned}\kappa_{\alpha,\beta}^{HTC} &= \frac{\hbar^2}{N_r V_{puc} k_B T^2} \frac{1}{N_i} \sum_{i=1}^{N_i} \int_0^\infty dt \sum_{\mathbf{K}, J}^{Cuboid} (\Omega^{(i)}(\mathbf{K}, J))^2 \mathbf{V}_{puc}^{(i)\alpha}(\mathbf{K}, J) \mathbf{V}_{gr}^{(i)\beta}(\mathbf{K}, J) \\ &\quad \times (n^{(i)}(\mathbf{K}, J) + 1) (n^{(i)}(\mathbf{K}, J) \times \frac{1}{2} \cos[2(\Omega^{(i)}(\mathbf{K}, J) - \Omega^{(0)}(\mathbf{K}, J))t])\end{aligned}\quad (37)$$

where  $N_i$  is the number of DET - deformed elastic tensors,  $V_{puc}$  volume of the primitive unit cell. The *Cuboid*, see Fig. 8 is a volume in the reciprocal zone, with center point at  $\mathbf{K} = \mathbf{0}$ . In LTC Eq.(21), the summations  $\sum_{\mathbf{k}, j}$  run homogeneously over the whole Brillouin zone. In HTC Eq.(37), the summations  $\sum_{\mathbf{K}, J}$  should run over small wavevector volume around  $\mathbf{K} = \mathbf{0}$  as indicated in Cuboid,  $\sum_{\mathbf{K}, J}^{Cuboid}$ . The central green box should always remain empty (it is direct space beyond volume of the sample), so there no wavevectors should be positioned. In the volume of the larger inner box (between green and red boxes), the wavevectors  $\mathbf{K}$  for elastic waves should be placed. Notice, that a lot of wavevectors can determine crystal phonons, much less wavevectors are indexing the elastic waves. The central box excludes such long wavevec-

where  $\mathbf{i}, \mathbf{j}, \mathbf{k}$  are versors along  $x, y, z$  directions.

Max Born developed in his book<sup>55</sup> a method which correlates the elastic constants with the slopes of acoustic phonon modes at a particularly small wavevectors. As a matter of fact, the elastic waves have been identified as the acoustic waves at small  $\mathbf{K}$ . Therefore, expression for LTC thermal conductivity should hold for HTC, with only a few differences listed below.

The lattice thermal conductivity calculations introduced above for phonons can also be used for elastic waves. Although their wavelengths are evidently longer than the size of the supercell used in *ab initio* calculations, one may account the long wavelength doing the following: (i) create phonon displacement patterns DP in conventional supercells, for example the same as for phonons, (ii) see that the displaced atoms also cause changes of the elastic constants, (iii) call *deformed elastic tensor* (DET), which conventionally will be the supercell deformed itself, what results in symmetry lowering to DET.

By solving now the Cristoffel equation, Eq.(32),<sup>60</sup> with DET, one calculates the elastic wave frequencies, finding their frequency changes with respect of ideal supercell tensor. One may say that the Cristoffel equation rebuilds the ideal elastic wave to whole space from the crystal segment belonging to DET limited to studied supercell. Moreover, the group velocities Eq.(36), can also change. These changes influence the relaxation time of conducting objects acting in thermal conductivity.

The relation for high thermal conductivity (HTC) formulated in analogy with lattice thermal conductivity LTC, Eq.(21), for the simulation with the deformed elastic tensor DET reads

tors  $\mathbf{K}$ , which surpass the sample macroscopic size, or the mean distance between boundaries existing in the media. In general, the wavevectors should be places at random, unless the wavevectors amplitudes and positions express some superstructure being a new object of the study. Then, the positions and amplitudes of wavevectors  $\mathbf{K}$  could be derived from the object in the direct space and then transformed to the cuboid by three-dimensional Fourier transform. Of course, the shape of the Cuboid may change to adapt to the studied object. Remember that sets of wavevectors for phonons  $\mathbf{k}$  and elastic waves  $\mathbf{K}$  are needed for LTC Eq.(21) and HTC Eq.(37) expressions, respectively. And that the HTC must be described by wavevectors from the elastic wave region.

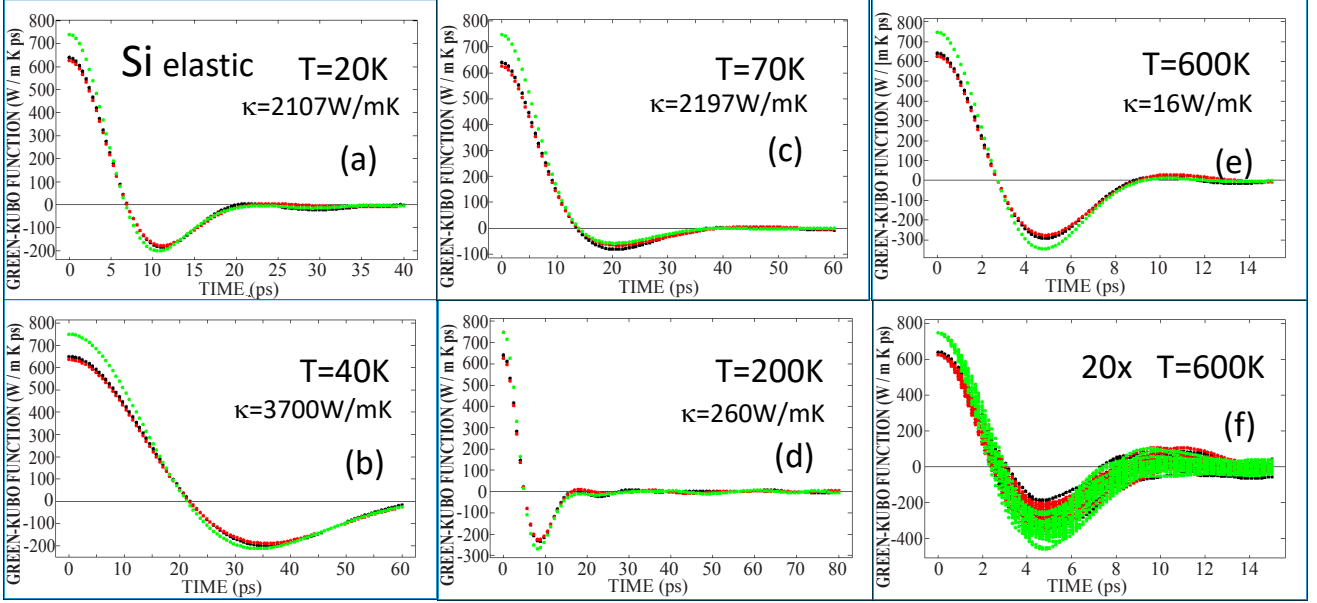


FIG. 9. Silicon Si. (a,e) HTC averaged Green-Kubo functions calculated from Eqs(37) and (26), (f) Green-Kubo functions for HTC (elastic waves) calculated directly from Eq.(37). Each run used 20 DET.

## B. Silicon HTC

To calculate the HTC of silicon the formulae for thermal conductivity Eq.(37) was used. The 20 DP were prepared for each  $T = 7, 20, 40, 70, 200$  and  $600K$ , and then 20 DET's were created in each case. During heating the lattice constants and pressure stayed constant as observed for LTC of Si. The elastic tensors, called also elastic modulus, were calculated on VASP<sup>47,56</sup>. One must also add that the cpu calculation time of this process is long in comparison to cpu run for elastic tensor possessing some symmetry elements. It is a result of the fact that the DET's do not have any symmetry, hence, it requires to calculate much more iterations.

Moving back to HTC, one should supply some information on the crystal microstructure, and include it to Eq.(37). The minimum information should indicate the possible range of the wavelengths of the elastic waves before they reach the boundaries, which hinder their travel and then determine the expected HTC. In the present stage of the current theory we may propose to select the proper wavelengths, or rather wavevectors of the elastic waves only, and check whether they lead to correct results observed in experiments. The idea is that the shortest wavelengths  $\lambda_{min} = 2\pi/K_{max}$  of the elastic waves start from a distance just above the active wavelength of low frequency of acoustic phonons, and spreads to longest distances to "boundaries"  $\lambda_{max} = 2\pi/K_{min}$ . It is expected that elastic waves characterized by wavevectors  $\mathbf{K}$  from the interval  $\mathbf{K}_{min} < \mathbf{K} < \mathbf{K}_{min}$  could propagate in the crystal without obstacles. Generally, such precise information is missing. Moreover, the crystal microstructure may depend on distributions of the boundaries within the crystal, microcracks, kind of defects and impurities, etc. and as such they ought to be a topic of separate study. Here, the volume of the perfect crystal

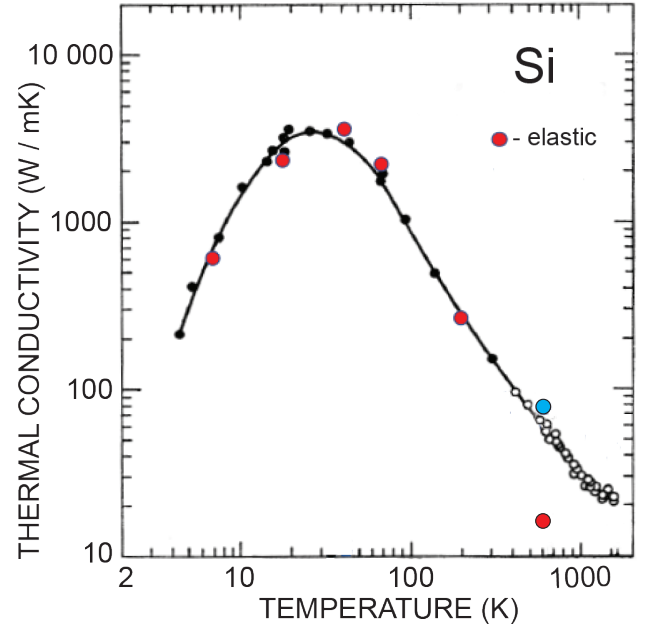


FIG. 10. Silicon Si. (red) Calculated HTC data using Eq.(37) making use of elastic waves. (blue) Single point of LTC data at  $T = 600K$ , imported from Fig. 5. (black) Measured thermal conductivity from Ref.<sup>25</sup>.

is represented by a cuboid, Fig. 8 filled with the wavevectors  $K$  with an exception of the inner box, which should be empty. In the direct space the empty box represents the outer part beyond the crystal and the cuboid represents surface layers of the real crystal, expected to suppress propagation of elastic

waves.

In the present stage of the theory the microstructure information could be accounted in a primitive way, namely by limiting the boundary to select the wavevectors  $\mathbf{K}$  belonging to cuboid in the summation  $\sum_{\mathbf{K},J}^{Cuboid}$  of the formula Eq.(37). For the present study of Si, the random wavevectors were selected out the volume of the cuboid confined by minimal value  $\mathbf{K}_{min} = 0.00001\text{\AA}^{-1}$  to maximal value of  $\mathbf{K}_{max} = 0.030\text{\AA}^{-1}$ . The inner box inside  $\mathbf{K}_{min} = 0.00001\text{\AA}^{-1}$  was left empty. The wavevectors  $\mathbf{K}_{max}$  and  $\mathbf{K}_{min}$  correspond to the lengths of elastic waves from  $0.021\mu\text{m}$  to  $63\mu\text{m}$ , respectively. Since in the cuboid the wavevectors distribution is homogeneous the amount of elastic waves taken in derivation of the HTC close to  $63\mu\text{m}$  is less than in vicinity of  $0.021\mu\text{m}$ .

The above mentioned summation in the cuboid was used to compute the Green-Kubo functions. The selected function are shown on Fig.9. The vertical axes of plots are mainly determined by the group velocities and temperature occupation distributions and they stay almost constant. But the horizontal axes cover changeable time intervals. Thus, time seems to decide about the magnitude of the relaxation times and thermal conductivities. In particular after initial maximum at  $t = 0$ , the Green-Kubo function diminishes to negative minimum. Such a decrease is caused by the difference of two cosines occurring in the relaxation time expression, Eq.(37). Namely, small differences between the elastic wave frequencies of deformed and perfect supercells lead to minimum at longer times, in contrary to opposite situation with large frequency difference and the minima occurring at shorter times. The Green-Kubo functions accompanied the elastic waves can be seen on the plots. The minima of the (a-f) plots are drawn from 20 runs of DET's. On (f) all 20 plot are seen and some smearing of the data are observed.

Relation Eq.(37) gives also the numerical value of thermal conductivity as a function of temperature. For silicon the low temperature HTC results are plotted on Fig.10 The LTC data reaches maximum  $96.8W/mK$ , while the HTC is elevated to  $3700W/mK$ . This high difference is mainly caused by the increase of the global relaxation times in HTC mechanism. Longer relaxation times result in higher values of  $\kappa_{\alpha,\beta}$ . The silicon single crystal, for the HTC measurements by Glassbrenner and Slack reported in<sup>25</sup> and used for the low-temperature measurements, was grown from high-purity silicon. The growth process was made with care in order to make the crystal to be oxygen and dislocation free. Then, any vacancy clusters were less than one micron in diameter. The sample boundary sizes were not reported.

It is worth to mention that at low temperature the occupation factor  $(\frac{\omega}{T})^2(n(\frac{\omega}{T}) + 1)n(\frac{\omega}{T})$  in Eq.(37) reduces the intensity of the Green-Kubo function. These properties also force to decrease HTC close to  $T = 0K$  to a very small value. With increasing temperature the mentioned thermal factors approach 1. Similar effect has been seen for MgO.

TABLE III. Silicon Si and Magnesium Oxide MgO. Calculated averaged sums  $\frac{1}{3}(\kappa_{1,1} + \kappa_{2,2} + \kappa_{3,3})$  of the high thermal conductivities Eq.(37), and the global relaxation times, Eq.(29).

Si $T(K)$	7	20	40	70	200	600
$\kappa(W/mK)$	628	2107	3700	2197	260	21.2
$\tau(ps)$	29.6	21.6	20.7	10.4	1.63	0.11
MgO $T(K)$	5	25	40	100	300	
$\kappa(W/mK)$	514	3225	2932	218	0.14	
$\tau(ps)$	1.15	9.94	8.81	8.36	0.13	

### C. Magnesium Oxide HTC

To calculate the HTC of magnesium oxide, MgO atomic displacements DP were prepared for each  $T = 5, 25, 40, 100$  and  $300K$  and next 20 DET's tensors were created for each  $T$  using VASP. During heating the lattice constants and pressure behaved as observed for LTC of MgO.

The below mentioned summation within the cuboid was used to compute the Green-Kubo functions. The selected functions are shown on Fig.11. The vertical plot axes are mainly determined by the group velocities and temperature occupation distributions and they stay almost constant. But the horizontal axes cover changeable time intervals. Thus, time seems to decide about the magnitude of the relaxation times and thermal conductivities.

To calculate HTC of MgO one should select data for the cuboid. The following wavevectors have been proposed: maximal values of  $\mathbf{K}_{max} = 0.0030\text{\AA}^{-1}$  and minimal value of  $\mathbf{K}_{min} = 0.00001\text{\AA}^{-1}$ . The selected cuboid wavevectors for MgO correspond to boundaries of the elastic waves being in the range from  $0.21\mu\text{m}$  to about  $63\mu\text{m}$ , respectively. This information was used in Eq.(37) to compute the time dependent Green-Kubo HTC functions, and later plotted on Fig. 11. The HTC data reaches maximum  $3700W/mK$ , The variation of the HTC in MgO are presented on Fig.12. The  $T = 5, 25, 40, 100K$  fit to measured data, but the contribution of HTC at  $T = 300K$  practically vanishes. At  $T = 300K$  only LTC contributes.

The two approaches provide thermal conductivity LTC and HTC. Therefore, it rises a question what happens in the temperature interval between the LTC and HTC regions. The present results give for *Si* at  $T = 600K$ : HTC:  $21, 2W/mK$ , LTC:  $84W/mK$  Exp: $84.5W/mK$ , and for *MgO* at  $T = 300K$ : HTC:  $0.14W/mK$ , LTC:  $110W/mK$  Exp:  $75W/mK$ . This means that LTC mechanism is used at higher  $T$  and then at lower  $T$  it became replaced by HTC processes. Probably, this effect occurs in special materials only.

### D. Microstructure in HTC

The current approach relates the HTC and microstructure in the region of low temperatures. The conventional process to carry on the HTC calculations would be to look into cuboid for the wavevectors data to get an agreement between calculated

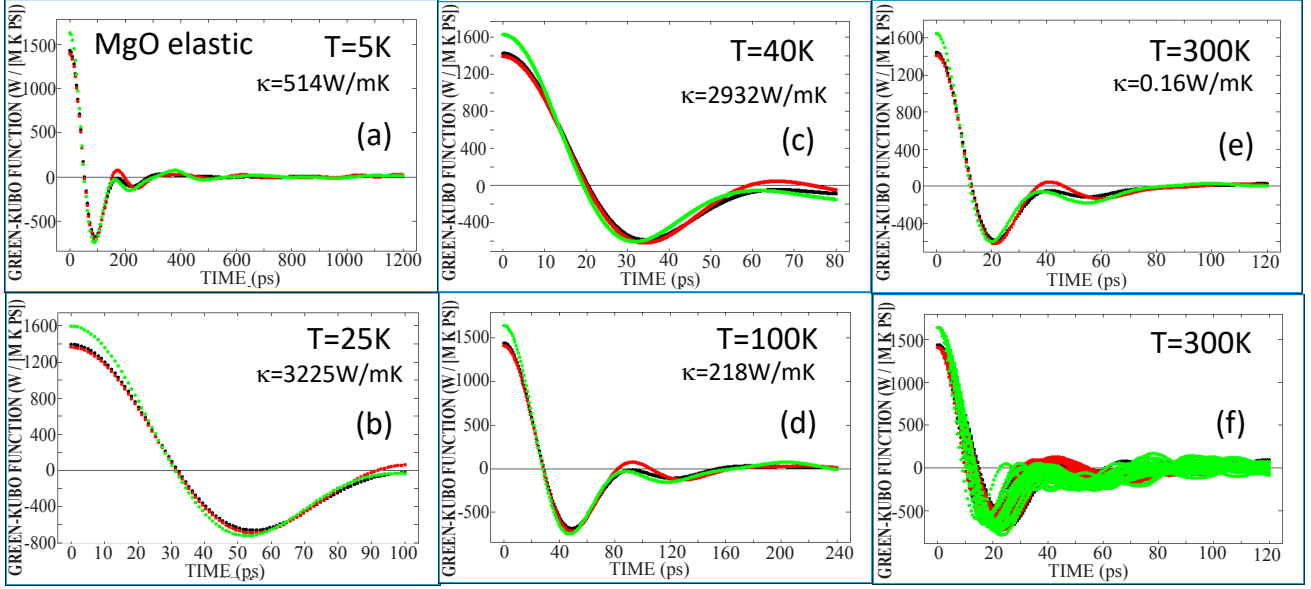


FIG. 11. Magnesium oxide, MgO. (a,e) HTC averaged Green-Kubo functions calculated from Eqs(37) and (26), (f) Green-Kubo functions for HTC (elastic waves) calculated directly from Eq.(37). Each run used 20 DET.

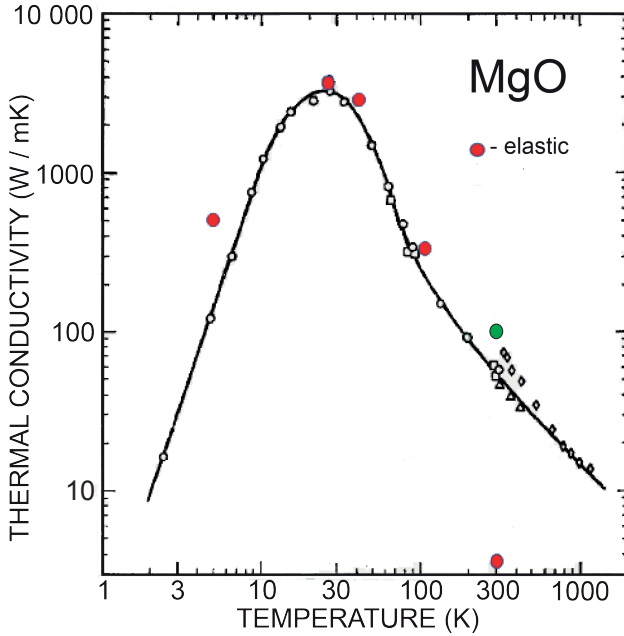


FIG. 12. Magnesium oxide, MgO. (red) Contributions of only elastic waves to high thermal conductivity. (green) Single point of LTC data at  $T = 300K$ , imported from Fig.7. (black) Experimental points from<sup>22</sup>

and measured  $\kappa_{\alpha,\beta}^{HTC}$ . It would mean to find right values of the wavevectors inserted to cuboid. However, the reverse process would be more valuable. First the microstructure features are foreseen and used to modify the cuboid, and next to collate the

calculated data with the behaviour of the measured HTC. In this case the method could have some predictive power, which might help to design the required properties of the material, say microstructure.

As a test we have inserted to the cuboid of Si crystal being at  $T = 40K$ , the wavevectors of  $\mathbf{K}_{min} = 0.00001 \text{ \AA}^{-1}$  and  $\mathbf{K}_{max} = 0.00015 \text{ \AA}^{-1}$ , corresponding to Si boundary distances from 63 and 4.2  $\mu\text{m}$ , respectively. For these wavevectors HTC tremendously increases the global relaxation time to 1700  $ps$  and thermal conductivity to  $\kappa_{\alpha,\beta}^{HTC} = 320000W/mK$ . Other obstacles might diminish/change this value.

Presently the cuboid volume is filled with wavevectors of the same amplitude. However, having a concept of the microstructure of considered crystal one might convert this information to the amplitudes of wavevectors placed in the cuboid. Such a project is still waiting for realization.

There are many studies, which need to combine the microstructure of the sample with its thermal conductivity. Here, follows some example (1) The thermal energy transport in actinide oxide nuclear fuel materials<sup>57</sup>, thorium dioxide and uranium dioxide. The first has a characteristic maximum of thermal conductivity below 40 K. The second has a reduced thermal conductivity, in spite of similar crystal symmetries. It happens due to the presence of elastic phase transition. (2) The dislocation impact on thermal conductivity<sup>58</sup>. Dislocations induce the stress field, which might lead to anisotropy of thermal transport. Such a contribution can be estimated. Another goal would be to analyze the collection of dislocations on thermal conductivity. (3) Thermal properties of the superelastic, which consist of many crystal variant of shape memory alloys (as NiTi). The complex microstructure exists due to well-known compatible equations for pair of crystals variants, which require to identify the interfaces<sup>59</sup>.

The MD simulations of simple crystal models have shown that realistic microstructures of  $YBa_2Cu_3O_7$  superconductor<sup>61</sup> and  $LaNbO_4$  ferroelastic<sup>62</sup> could be obtained starting from a simple crystal model at relatively high temperature, and next quenching. The simulated microstructures and those obtained from TEM observations are very similar. It is also worthwhile to mention the effort to increase effectiveness of thermoelectric  $CaCd_2Sb_2$ <sup>63</sup>. It has been proposed to replace  $Cd$  by  $Mg$ , as point defect, to induce significantly phonon scattering, but maintaining the carrier concentration, lower essentially their LTC and increase figure of merit  $ZT$ .

## V. CONCLUSIONS AND DISCUSSIONS

The mechanisms of thermal conductivities discussed in this article is based on the anharmonic phonons formalism handled within the non-perturbative approach for crystals,<sup>30</sup>. Due to it, the formulated theories of LTC and HTC have been retrieved starting from different and not conventional anharmonic approaches. In the LTC case phonons play a role of the heat transport media realized by anharmonic phonons of the crystals. The anharmonic vibrations of atoms determine the crystals temperature. Next, one prepares several displacement pattern DP of atoms in the crystal supercells, with amplitudes displaced corresponding to studied temperature. Then, the forces induced by the displaced atoms are calculated with the *ab initio* software, which permits to solve the set of lattice dynamics equations, and find information about the harmonic and anharmonic interatomic potentials. This technique has been successfully used to create positions, shifts, widths and shapes of anharmonic peaks and determine the analytical expression for the mode relaxation times for all anharmonic modes without performing expansion of the interaction potential over anharmonic terms and without using the Boltzmann equation. Specially, the relaxation times could be calculated analytically, and this process needs only to know the differences of anharmonic and harmonic frequencies for each segment of the anharmonic phonon mode belonging to the same  $(\mathbf{k}, j)$  phonon mode.

Some crystals require to take into account also the elastic waves, which need to be considered within different mathematical formalism. The elastic waves, travel in the crystal and form a strain variation of predefined units of crystal, usually supercells. Atomic displacement patterns, similar to those of phonons, create some strains, deform supercells, and hence create the elastic waves. Finally, the elastic waves can be found by solving the Cristoffel equation, being entirely defined by the elastic constant tensors.

We have shown that the crystal thermal conductivity is determined by the Green-Kubo relationship being the correlation function of the heat flux. The high thermal conductivity can be calculated from products of elastic wave frequencies, elastic wave group velocities, and phonon relaxation times specific for elastic waves.

Second essential difference between lattice and high thermal conductivity is related with the wavevectors summation within the correlation functions. In the phonon part all

wavevectors need to be used in the sum over the Brillouin zone. The elastic waves are characterized by very long wavelengths, so only the short wavevectors around  $k = 0$  and lower than  $1 - 4THz$  participate in the thermal conductivity. This effect is applied to fix the longest wavevectors as being able to reach the sample sizes, or other obstacles which limit the transport of the elastic waves. This criterion leads to statement that the calculated HTC may agree with the measurements. To facilitate the procedure to limit the used wavevectors for the elastic wavevectors, the cuboid of  $3d$  figure was introduced. In future the cuboid might also allow to study thermal conductivity of crystals with defects, microstructure, etc.

## ACKNOWLEDGMENTS

The author would like to acknowledge Dr Erich Wimmer and Dr Walter Wolf from Materials Design Inc for suggestions and fruitful discussions.

## AUTHOR DECLARATIONS

### Conflict of Interests

The author has no conflict to disclose.

## DATA AVAILABILITY

The data that support the findings of this study are available within the article.

## REFERENCES

- <sup>1</sup>G.P.Srivastava, in *High Thermal Conductivity Materials*, edited by S.L.Shindé and J.S.Goela. (Springer Science Business Media, Inc. New York, 2006). p.1.
- <sup>2</sup>R.A.Cowley, Rep. Prog. Phys. **31**, 123 (1968).
- <sup>3</sup>A.A.Maradudin, and A.E.Fein, Phys.Rev. **128**, 2589 (1962).
- <sup>4</sup>K.H.Michel, S.Costamagna, and F.M.Peeters, Phys.Rev. B **91**, 134302 (2015).
- <sup>5</sup>P.Scuracchio, K.H.Michel, F.M.Peeters, Phys.Rev. B **99**, 144303 (2019).
- <sup>6</sup>T.H.K.Barron, and M.L.Klein, in *Dynamical Properties of Solids*, edited by G.K.Horton, and A.A.Maradudin (North-Holland, Publishing Company, Amsterdam, American Elsevier Publishing Company, Inc, New York, 1974) Vol. 1, p. 391.
- <sup>7</sup>G.Deinzer, G.Birner, and D.Strauch, Phys.Rev. B **67**, 144304 (2003).
- <sup>8</sup>K.Esfarjani, and H.T.Stokes, Phys.Rev. B **77**, 144112 (2008).
- <sup>9</sup>T.Tadano, and S.Tsuneyuki, J. Phys. Soc. Jpn. **87**, 041015 (2017).
- <sup>10</sup>G.Grimvall, *Thermodynamical Properties of Materials* (Ansterdam, Lausanne, New York, Oxford, Shannon, Singapur, Tokyo, Dover, New York, (1999).
- <sup>11</sup>J.Callaway, Phys.Rev. **113**, 1046 (1959).
- <sup>12</sup>A.Ward, D.A.Broido, D.A.Stewart, G.Deinzer, Phys.Rev. B, **80**, 125203 (2009).
- <sup>13</sup>D.S.Kim, O.Hellman, N.Shulumba, C.N.Saunders, J.Y.Y.Lin, H.L.Smith, J.E.Herriman, J.L.Niedziela, D.L.Abernathy, C.W.Li, and B.Fultz, Phys.Rev.B **102**, 174311 (2020).
- <sup>14</sup>O.Hellman, I.A.Abrikosov, and S.I.Simak, Phys.Rev. B **84**, 180301 (R) (2011).
- <sup>15</sup>O.Hellman, I.A.Abrikosov, Phys.Rev. B **88**, 144301 (2013).



- <sup>16</sup>C.Carbogno, R.Ramprasad and M.Scheffler, *Phys.Rev.Lett.* **118**, 175901 (2017).
- <sup>17</sup>A.France-Lanord, P.Soukiassian, C.Glatli and E.Wimmer, *Phys.Rev.Appl.* **7**, 034030-1 (2017).
- <sup>18</sup>BinWei, Qiyang Sun, Chen Li, and Jiawang Hong, *Science China, Physics, Mechanics & Astronomy*, **64**, 117001 (2021).
- <sup>19</sup>I.Errea, M.Calandra, and F.Mauri, *Phys.Rev. B* **89**, 064302 (2014).
- <sup>20</sup>L.Monacelli, R.Bianco, M.Cherubini, M.Calandra, I.Errea and F.Mauri, *J.Phys.: Condens. Matter* **33**, 363001 (2011).
- <sup>21</sup>G.A.Slack, *J.Phys.Chem.Solids* **34**, 321 (1973).
- <sup>22</sup>G.A.Slack, *J.Phys.Rev.* **126**, 427 (1962).
- <sup>23</sup>E.K.Sichel, R.E.Miller, M.S.Abrahams, and C.J.Buiocch, *Phys.Rev.B* **13**, 4607 (1976).
- <sup>24</sup>M.G.Holland, *Phys.Rev.* **132**, 2461 (1963).
- <sup>25</sup>C.J.Glassbrenner and G.A.Slack, *Phys.Rev.* **134**, A1058 (1964).
- <sup>26</sup>K.Esfarjani, G.Chen and H.T.Stokes, *Phys.Rev.B* **84**, 085204 (2011).
- <sup>27</sup>T.Sun, X.Shen, and P.B.Allen, *Phys.Rev.B* **82**, 224304 (2010).
- <sup>28</sup>T.Sun and P.B.Allen, *Phys.Rev.B* **82**, 224305 (2010).
- <sup>29</sup>L.Isaeva, G.Barbalinardo, D.Donadio and S.Baroni, *Nature Communications* **10** (1), 1-6 (2019).
- <sup>30</sup>K.Parlinski, *Phys.Rev. B* **98**, 054305 (2018).
- <sup>31</sup>K.Parlinski, Conference Proceedings 479, "Neutrons and Numerical Methods" - N2M edited by M.R.Johnson, G.J.Kearley and H.G.Büttner, *Am.Inst.Phys.* p.121 (1999); *J. Phys.: Conf. Ser.* **92** 012009 (2007).
- <sup>32</sup>K.Parlinski, Z.Q.Li, and Y.Kawazoe, *Phys.Rev.Lett.* **78**, 4063 (1997).
- <sup>33</sup>G.Kresse, J.Furthmüller, and J.Hafner, *Europhys. Lett.* **32**, 729 (1995).
- <sup>34</sup>W.H.Press, S.A.Teukolsky, W.T.Vetterling and B.P.Flannery, in *Numerical Recipes* (Cambridge University Press, Cambridge, England, 1992), p.670.
- <sup>35</sup>P.Debye, *Ann.Phys.* **348**, 49 (1913).
- <sup>36</sup>H.Ott, *Ann.Phys.* **415**, 169 (1935).
- <sup>37</sup>N.W.Ashcroft and N.D.Mermin, Chapter 25, *Solid State Physics*, HRW International Editions, CBS Publishing Asia Ltd (1976).
- <sup>38</sup>AA.A.Maradudin, *J.Am.Chem.Soc.* **86**, 3405 (1964)
- <sup>39</sup>F.R.Gantmacher, *Applications of the theory of matrices*, p 53, (Wiley-Interscience, New York, 1959).
- <sup>40</sup>M.S.Green, *J.Chem.Phys.* **22**, 398 (1954).
- <sup>41</sup>R.Kubo, *J.Phys.Soc.Jpn.* **12**, 570 (1957).
- <sup>42</sup>R.Kubo, M.Yokota, and S.Nakajima, *J.Phys.Soc.Jpn.* **12** 1203 (1957).
- <sup>43</sup>R.J.Hardy, *Phys.Rev.* **132**, 168 (1967).
- <sup>44</sup>R.Zwanzig, *Ann.Rev.Phys.Chem.* **16**, 67 (1965).
- <sup>45</sup>G.P.Srivastava, *The Physics of Phonons* (Taylor and Francis, London 1990).
- <sup>46</sup>M.Kaviany, *Heat Transfer Physics* (Cambridge University Press, 2008).
- <sup>47</sup>G.Kresse, and J.Furthmüller, *Phys.Rev. B* **54**, 11169 (1996).
- <sup>48</sup>E.B.Christoffel, *Ann.Mat.Pura Appl.* **8**,193 (1877).
- <sup>49</sup>H.B.Huntington, in *Solid State physics*, edited by F.Seitz and D.TurnBull (Academic Press Inc. Publishers, New York, 1958), Vol. **7**, p.213).
- <sup>50</sup>Ph.Boulanger and M.Hayes, *Proc. R. Soc. London A* **454**, 2289 (1998).
- <sup>51</sup>M. H. F. Sluiter, M. Weinert, Y. Kawazoe, *Europhysics Letters* **43**, 183, (1998).
- <sup>52</sup>J.W.Jaeken and S.Cottenier, *Computer Physics Communications*, **207**, 445-451 (2016).
- <sup>53</sup>P.G.Klemens, *Thermal Conductivity and Lattice Vibrational Modes, Solid State Physics*, vol.7. p.1, (Academic Press Inc., New York, 1958).
- <sup>54</sup>F. I. Fedorov, *Theory of elastic waves in crystals*, Springer, (1968).
- <sup>55</sup>M.Born and K.Huang, *Dynamical Theory of Crystals Lattices* Oxford at the Clarendon Press 1954.
- <sup>56</sup>Y.Le Page and P.Saxe, *Phys.Rev. B* **65**, 104104 (2002).
- <sup>57</sup>D.H.Hurlay et al, *Chem. Rev.* **122**, 3711 (2022).
- <sup>58</sup>Y.Cheng, M.Nomura, S.Volz and S.Xiong, *J.Appl.Phys.* **130**, 040902 (2021).
- <sup>59</sup>Min-Jyun Lai, Hyng-Yuan Lu and Nien-TiTsou, *Multiscale Science and Engineering*, **1**, 141-149 (2019).
- <sup>60</sup>K.Parlinski, PHONONA software (2020).
- <sup>61</sup>K.Parlinski, Y.Watanabe, K.Ohno and Y.Kawazoe, *J.Mater.Res.* **10**,1864, (1995).
- <sup>62</sup>K.Parlinski, Y.Hashi, S.Tsunekawa and Y.Kawazoe, *J.Materials Research* **12**, 2428, (1997).
- <sup>63</sup>Z. Zhang, H.Yao, X.Jia, X. Wang, X.Li, C. Chen, X. Lin, J. Sui, X. Liu, J. Mao, G. Xie and Q. Zhang, *Appl.Phys.Lett.* **120**, 041901 (2022).